POLITECNICO DI TORINO

Corso di Laurea in Ingegneria Aerospaziale

Tesi di Laurea Magistrale

Development of an experimental test bench for the validation of prognostic algorithms for electromechanical actuators

Relatori:
Matteo Davide Lorenzo DALLA VEDOVA
Paolo MAGGIORE

Correlatore:
Pier Carlo BERRI

Tesi di Laurea di:
Leonardo BALDO

A mia nonna Rosella e a mio zio Franco,
senza i quali non sarei diventato
la persona curiosa
e desiderosa di conoscenza che sono oggi.

Contents

List of Figures

List of Tables

Abstract

This experimental thesis aims to develop and set up a total of two test benches concerning the validation of *Simulink* prognostic models.
De facto, in the context of this thesis, I have worked on two main topics:

1. an upgrade of a pre-existent experimental test bench with the aim of studying mechanical plays consequences on an additive manufacturing based planetary gearbox assembly;

2. the design and production phases of a different test platform, concerning fatigue implications on planetary gearboxes performance models.

The modelling, testing and research has been carried out with eng Luca Boggio and dr. eng. Matteo Bertone with the indispensable help of eng Pier Carlo Berri. The practical testing took place in a facility inside DIMEAS department, where the first experimental test bench is located. The first test platform had been realised by eng Pier Carlo Berri, eng. Pietro Sciandra and eng. Valentina Boschetti in the context of their thesis whereas further safety measures were put into place afterwards.

The first part of this document covers the work we have carried out together to set the test bench up for the tests. The final achievements, along with graphs, model validations and data processing results can be seen in eng Luca Boggio and dr. eng. Matteo Bertone theses whereas I will cover the test bench reshaping from a more practical perspective.

In the second part of the thesis the design and development process for the second test bench is reported.

In fact the thesis is divided into four main chapters: after a short introduction where the importance of modelling and the current state-of-the-art brushless technologies are examined, the paper goes on with the description of the first test bench and the modifications we implemented. After that, a profuse number of pages focuses on the design process concerning the second test bench. A chapter with final considerations and future developments is then reported.

Finally, two appendixes are present at the end of the project. The first one briefly shows some design iterations concerning the second test platform, while the last appendix displays a parallel work carried out in the first weeks of work at DIMEAS facility.

Nevertheless, the results showed in this work are of great value as they are suitable for an industrial use of Electromechanical Actuators too; for instance when installed over a vast kind of machinery (e.g. CNC machines). Moreover, given the low number of experimental databases for EMA, these platforms could provide extensive data sets enhancing industrial prognostic capabilities.

Chapter 1

Introduction

1.1 The relevance of models: EMA prognostic implementations.

The development and validation of models is nowadays an essential part of an aware, forward-looking design as well as a vastly widespread field of research in every scope of science and engineering. Especially in aerospace engineering solutions, where prototypes are expensive and testing conditions might be difficult to accomplish, the reliance on models, often integrated in more complex multi parameter environment (e.g. Digital Twins or BDAs), pervades every step of design, testing and support operations.
In fact prognostic algorithms capable of detecting potential failures before they can lead to extended and threatening failure conditions can assist the vehicle or the infrastructure in which actuators are used well after the design and production phases [18].
Being able to test extensively and feel the most subtle change in vibrations, power consumption, current, voltage and noise of electromechanical actuators could save an enormous amount of money, time and, more importantly, human lives.
Nevertheless, this kind of algorithms could be useful in maintenance operations resulting in the reduction aircrafts as well as industrial machines down-time, implementing more than ever the concept of *on-condition* maintenance, so welcomed by airplane handlers. In fact, with the help of Built In Test Equipment (BITE) and accurate and tailored algorithms, the overall maintainability of the product could rise even more, with the result of increased availability at lower costs [31, 43, 18].
Nowadays, with the increasingly higher demand of vehicles and aerospace components, engineers are asked to design optimum parts with low costs on all their life cycle. That is why, apart from the safety goals the implementation of these algorithms could offer, a strong reduction of Life Cycle Costs could be on the horizon, leading to a even more drastic cut to maintenance costs due to periodic checks.
A real time integrated aircraft and industrial health monitoring system could sets its root on these kind of algorithms, providing an all-in-one solution for prognostics issues and monitoring checks [31].

All things considered, the scope of this thesis is well set into the bigger framework of new aerospace technologies and philosophies. Among other aspects, the

aviation world is rapidly evolving into a *"more electric"* world with the newborn Boeing B787 as a forefather for More Electric Aircrafts (MEAs) [32, 34, 35].
The thesis work, focused on an electromechanical actuators (EMAs), is spot on and shows how EMAs can be an valid alternative to electrohydraulic actuators (EHA) especially in the control of secondary flight controls, where the diffusion of EMAs as means of motion is already well more widespread than in every other aircraft mechanical application.
Over the years, EMAs passed from a second choice equipment to a concrete future possibility thanks to enormous advances in technology and materials. However they are still quite new in the panorama of actuators and they are still seen with a bit of concern regarding safety (e.g. with respect to EMC and the most critical fault modes). In other words, EMAs lack the knowledge base which is common for other actuator types, in particular regarding fault detection and prognosis [35]. This is why a real time monitoring system based on sophisticated algorithms is essential to guarantee and satisfy the expected safety standards, providing industries with a robust tool for certification purposes too.
In this sense, in recent years, the *"Prognostic and Health Management"* (PHM) method has been developed to estimate the Remaining Useful Life (RUL) of components or systems by comparing the real response of the operating component or system with the nominal response, provided by a reference model.
After that, according to the information gained, different decision-making procedures can be approached before the hidden failure could turn into catastrophic failure conditions [35].
PHM is, on the other hand, a very innovative approach to handle *Safe-Life* components, among which the actuators are one of the most complex subsystems: not only detecting and identifying faults but also tracking their progression. This method also traces back the advancing failure to physically meaningful system parameters, providing practical information at the ground maintenance facilities [26, 40].
Furthermore, thanks to this methodology, EMAs have been gaining increased acceptance as *safety-critical* actuation devices earning important roles in airplane subsystems.

1.2 State of the art of electrical actuation technologies.

As MEAs are drastically changing the aviation world from the inside, new actuation technologies see their light to fulfill newer requirements and to be compatible with a completely new electric system architecture. One of the main advancements in the electric motors panorama (already some years ago) was the introduction of brushless motors which resulted in several advances in terms of maintenance time, costs and general safety. In fact, they manage to overcome many limits linked to DC brushed motors [35, 28]:

- much less maintenance due to the absence of brushes which have to be changed regularly given the high wear due to the sliding contact with the rotor;
- higher efficiency (Increased torque per watt of power input) and higher torque to weight ratio;

- increased constructive reliability due to the absence of brush commutator segments;
- a drastic cut in EMC problems thanks to the removal of brush commutators which caused electric arcs and sparks;
- the possibility of placing these motors in a more various kind of environments (e.g. in presence of dust or corrosive agents, fire dangers and explosive particles but also places difficult to reach for maintaining purposes) always thanks to the elimination of carbon brushes;
- less vibration with resulting supports weight reduction and mechanical noise cutback;
- less overheating problems (better heat dissipation) and less rigid speed limitation;
- overall longer lifespan;
- Brushless DC motors can have a finer feedback controls to monitor and control the speed and torque.

On the other hand their drawbacks are:

- they need a brushless motor controller to provide each stator windings with the correct current trend;
- despite lower operating costs, much higher purchasing and set-up costs;
- they are dependent on power electronics and control strategies;
- medium inherent fault tolerance capability and minor resonance issues.

To sum up everything that has been stated so far, with regard to the electrical machine topology and its operative consequences, brushless motors appear to be the way to go, despite having a much higher price [28].
Notably, the elimination of carbon brushes has a drastic positive impact on almost every aspect of the motor: the brushes absence and the consequent elimination of ionizing sparks from the commutator helps in EMI, maintenance, costs, control strategies etc...
In aerospace engineering, common kinds of brushless motors are: *Brushless DC motors* (BLDCs) and *Permanent Magnet Synchronous Motors* (PMSMs).
Despite their names, they are both **permanent magnet brushless synchronous electric motors**.
They are both based on permanent magnets which generate the rotor magnetic field.
They are both designed without brushes and commutators.
This are both synchronous: the rotor normally rotates at an angular speed equal to that of the revolving magnetic field in the machine.
Usually, for big industrial purposes, they are three-phase motors, like the one mounted on the test bench.

The other main difference between brushed and brushless motors concerns the functions associated to the rotor and the stator: in fact the rotor houses the permanent magnets (divided into pole pairs) while the electromagnets are on the stator. In brushed motors they are reversed.
Rotation is achieved by changing the direction of the magnetic field generated by the surrounding stationary coils, powered by Motor Control Units (MCUs) which need to have a rotor position feedback. The rotor permanent magnets try to align its intrinsic magnetic field with the stator's one, which is rotating, providing magnetic and reactance torque and hence movement.
As already briefly said, with a brushed motor, rotation is achieved by controlling the magnetic fields generated by the coils on the rotor trough current transmitted with brushes, while the magnetic field generated by the stationary stator magnets remains fixed and constant.

Stators usually feature soft ferromagnetic material winded up with isolated copper wires. Soft ferromagnetic materials present rapid transformation of the magnetic field H into magnetic induction B (a very tight and narrow hysteresis cycle (Figure 1.1b)). In fact, since the role of the stator in a brushless motor is generating a rotating magnetic field, the material has to be easily magnetised granting a quick change in the magnetic induction vector every time a current switch is ordered.
The rotor consists of shaft and a hub with permanent magnets. These are, on the other hand, made out of a very hard ferromagnetic material since their function requires that its magnetic orientation doesn't change in time (Figure 1.1a).
As stated before, there are two main kinds of brushless motors used in industrial

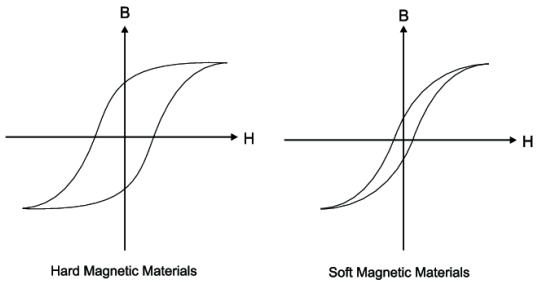

Figure 1.1: Hysteresis cycle for different magnetic materials.

aerospace applications: BLDC motors and, more often, PMSMs. They are quite similar motors as they share the same general structures and components. The main difference lies in the shape of the Back Electromotive Force EMF and controlled input current: trapezoidal for BLDC motors and sinusoidal for PSMS (Figure 1.2).
In fact, the main aim of of a motor is generating torque, which is desired constant at a specified working point and is a function of current and Back EMF.
The Back EMF, in turn, is a function of how the stator has been wound.
According to different winding strategies the BEMF can be trapezoidal or sinusoidal.
To accomplish a constant torque it is then clear that the injected current must be trapezoidal in BLDC and sinusoidal in PSMS.

After this brief explanation, the next paragraphs will look at their characteristics in more details as follows: main description, stator and rotor constructive principles, working principles and applications [28, 35, 38].

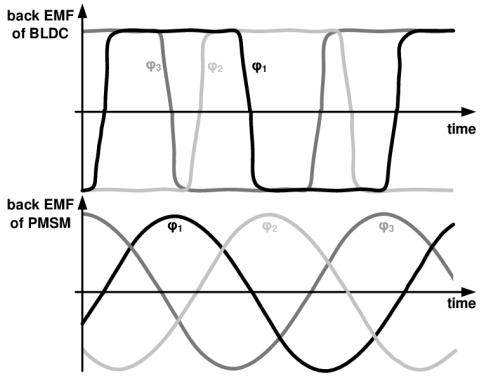

Figure 1.2: Different signal waveforms for a three-phase motor.

1.2.1 Brushless DC motors (BLDC)

Main description

BLDC motors are DC brushless motors characterised by a trapezoidal control. The main difference with respect to conventional DC motor is that the commutation is performed electronically by a controller rather than mechanically by brushes and commutators.
As a matter of fact, the windings are connected to a control circuit, which energizes each winding in a specific manner such that a rotating magnetic field is generated. As already stated, these motors, which require a DC input, are controlled with a trapezoidal control technique. This means that the DC input is switched from one stator coil to the next one to generate an AC voltage waveform with a trapezoidal shape on each winding. The same waveform is thus created also both for the current circulating within the motor phases and for the Counter ElectroMotive Force (CEMF). That being said, it goes without saying that, in contrast to ordinary brushed DC motors, BLDC requires a position feedback, commonly carried out through the use of hall sensors (usually embedded into the stator) or rotary encoders to manage the currents handling. This control technique, despite being one of the easiest control algorithms, causes some torque oscillations, which brings to poor performance at low speed regimes. Moreover, BLDC motors generally benefits from concentrated windings. This means that a single winding involves only one magnetic tooth, without overlapping between different windings. The result is a discrete switching between phases, with the resulting rotor magnetic field not always perpendicular to the stator one. This clearly is responsible for torque reduction and losses.

Constructive principles

- **Stator.** As explained before, stators are made up of soft ferromagnetic materials to provide a reduced hysteresis cycle with a rapid response. As usual in ferromagnetic cores, the parts are made up of several low thickness laminations of material to reduce eddy currents. Then,the steel plates in the stator can be slotted or slotless according to the specific motor (Figure 1.3).
  Slotless cores are characterized by a lower inductance, therefore the current

quickly energizes the electrical windings, allowing high accelerations and rapid dynamic response (useful for very high speed applications). However, usually the slotted option is the more widely used since the greater number of windings required to compensate for the absence of air gap in slotless stators means increased production costs with little advantages. It has to be recalled that many design requirements can influence the slotted or slotted choice in design phases, since the advantages and disadvantages of each solution are many but they are beyond the scope of this thesis. Finally, the stator, in conjunction with the rotor, manages to generate a nearly uniform flux density in the air gap.

Windings connections are usually achieved with a *star* or *delta* type of con-

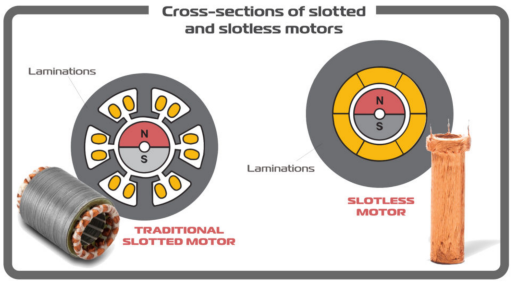

Figure 1.3: Slotted and slotless stators.

nections: in the first one the terminals of the three branches are connected to a common point, while in the second the terminals are connected in a closed loop (forming a delta shape). The consequences of one configuration or the other are profound and influence the phase voltage and current, speed, required insulation levels, number of wire turns, the existence of a common point... Usually, in modern motors the *star* configuration is the most common, since in the *delta* connection it is not possible to leave a phase without power supply: this gives intrinsic fault tolerance capability.

- **Rotor.** BLDC rotors are engineered with ferrous mixtures (ferrite magnets) rare-earth alloys (e.g. high-performance *Neodymium-Iron-Boron (NdFeB) alloys*). They are all hard ferromagnetic materials preferably with a high magnetic density which help in reducing the rotor size. Depending on the motor, the number of pair of magnets can vary between 2 and 8 alternating between north and south poles. The higher the number of magnetic pairs, the more regular is the obtained torque but also the more limited is the maximum angular speed. This is linked to the maximum switching frequency with many magnetic pairs. In any case, permanent magnets are arranged so that the magnetic field is always perpendicular to the motor surface.
  As for the stator, various kinds of rotors are present on the market: first of all the permanent magnets can be embedded or inserted well inside the rotor (*Interior-mounted PM rotor (I.P.M.)* also known as *anisotropic motors*) or placed on its surface (*Surface-mounted PM rotor (S.P.M.)* also known as *isotropic motors*) (Figure 1.4). Finally, the magnets can also be embedded in the rotor. I.P.M. are more suitable for higher angular velocities.

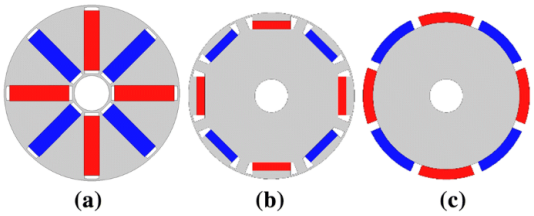

Figure 1.4: Different magnet placements: a,b) Interior-mounted; c) Surface-mounted

Secondly, there are *inner rotor mounted (Inrunner)* motors and *outer rotor mounted motors (Outrunner)* (Figure 1.5). The first type of motor place the stator on the outside with the rotor on the inside, while the second type place the stator on the inside with the rotor on the outside. As a consequence the first ones are usually longer with a smaller diameter than the others. Clearly, the first solution benefits from a better heat dissipation configuration and it is the most used in industrial applications. *Outer rotor mounted motors* have their application field for specific purposes thanks to a generally grater torque, generally smaller rotor inertia, larger air gap, smaller length but bigger radius.

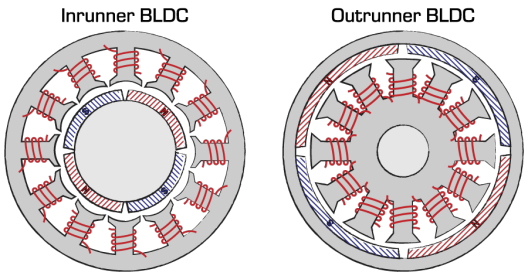

Figure 1.5: Different rotor placements.

Working principles and applications

To show the working principles of a BLDC motor, it is common to focus on a three phase slotted motor, frequently used in industrial applications. As already explained, the rotor motion is achieved through a rotating magnetic field, generated by the stator, which interacts with the permanent magnetic field of the rotor to accomplish a correct alignment between the two. In fact, their misalignment generates a torque which, applied to the rotor, generates a rotation.
In a 3-phase motor, three different signals are given to three (or more) windings coiled on ferromagnetic slots. The generation of signals is achieved through an inverter, which is responsible to switch the electric current from one winding to another, according to the rotation feedback of an encoder, of Hall sensors or, in a *sensorless* machine, through the variation in current and voltages.
When the current flows around one slot, a directional magnetic field is generated and, if it direction is not equal to the rotor permanent magnetic field one, a torque is generated too.
It is then clear that, if the excited windings change in time, the tendency of the

rotor is to follow the rotating magnetic field. As the rotor spins, the direction of the stator magnetic field has to be updated to keep the rotor turning. In addition, if the phase shift between the two magnetic field is 90°, the torque generated is at its maximum value. This is one of the flaws of BLDCs since, presenting a trapezoidal control, the rotation of the field cannot be very smooth, especially at low speeds.
For reasons of clarity, Figure 1.6 shows two subsequent steps in order to make the rotor rotate of 60°. The example depicts a 3-phase motor with 3 main slots (a simplified version), three Hall sensors and a solid state inverter. In realistic implementations more than three paired windings are present to generate a more uniform magnetic field. It can be noticed that, according to the Hall sensor readings (black dots or red dots) the correct winding is excited, enabling the two magnetic fields to be always in quadrature (in ideal conditions). The powering of different windings is often accomplished by a six-step commutation process inside the inverter.

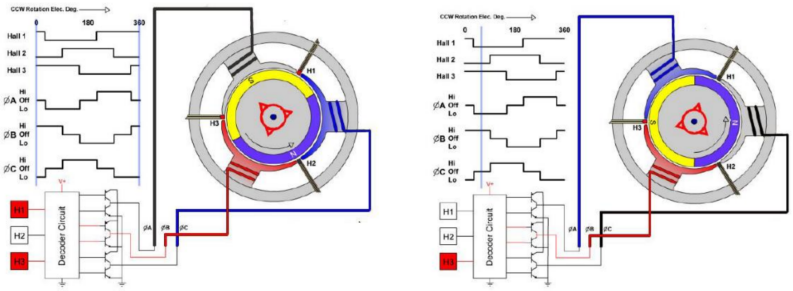

Figure 1.6: Two steps of rotation by means of current switching.

In conclusion, BLDC machines are especially interesting for high speed applications (given the problems at low speeds) and applications where a continuous rotation is needed (for instances electric power trains for electric vehicles). Minor disadvantages are strictly linked to the implemented trapezoidal algorithm: torque ripples, vibrations and slightly poorer performance than sinusoidal controlled motors, such as PMSMs. In fact, the phase switching causes a sudden interruption of the magnetic field; they are hence use where performance requirements are not too demanding.

1.2.2 Permanent Magnet Synchronous Machines

Main description

PMSMs are brushless motors characterized by a sinusoidal control. It is worth repeating that, being a brushless motor, PMSMs present the following architecture: the permanent magnets rotate and the conductor remain stationary.
PMSMs need to be commutated like BLDC motors but with more complex algorithms to achieve a smoother transition between phases and, hence, a smoother torque generation. As a matter of fact, this is accomplished by changing the control strategy from a trapezoidal one to a sinusoidal one and by minor changes to stators and rotors constructive strategies.
Contrary to BLDC motors, PMSMs exploits AC current and they usually require a

three phase AC electric signal. Each coil is powered by a sinusoidal voltage which is 120° out of phase from the signal sent to the other coils.
As already said, PMSMs are deemed an upgrade to BLDC motors since sinusoidal control manages to achieve a smoother and more fluid rotation even at low speeds, providing a more efficient solution in terms of torque generation.
In fact, the torque is continuous and almost constant, without annoying torque ripples typical of BLDC, while the back EMF presents a sinusoidal waveform.
For all intents, PMSMs can be seen as an hybrid mix from both BLDC motors and induction motors, since the sinusoidal flux density in the air gap resembles that of an induction motor while the installation of permanent magnets on the rotor is owned to BLDC motors.
This kind of motor usually controls the current in each winding trough a nowadays very common control strategy, PWM, better explained in the following paragraphs.
PMSMs require a position feedback, just like BLDC, since the three out-of-phase signal must be sent to each winding according to the rotor position to guarantee the optimum thrust generation.

As in BLDC motors, this is achieved trough various kinds of equipment: given the general high cost of PMSMs, more advanced technology can be approached and, usually, this translates to very precise encoders or hollow shaft resolvers. Resolvers, which exploit electromagnetic phenomena instead of optic ones, are better suited for harsher environments, typical of aerospace applications. In fact, despite having a little less precision, they are more robust and rugged, offering an ideal solution when high resilience over vibrations, accelerations or high temperatures. On the other hand, (optical) encoders are usually lighter, simpler, cheaper and presents less rotational inertia, very handy when they are subjected to high acceleration. Furthermore, encoders are quickly moving forward to more accurate measures, offering a wide range of possibilities.

To sum up everything that has been said so far, higher accuracy, smoother performance, higher torque, enhanced ruggedness and overall better performances lead to much higher costs for PMSM, though affordable for aerospace applications.

Constructive principles

- **Stator.** Stator technology varies slightly compared to BLDC motor building technology. In fact, they share the same materials: very soft ferromagnetic materials with high magnetic permeability to enhance the magnetic field are used. They also require very tight hysteresis cycle. All considerations proposed for BLDC are valid here too.
  The main difference, in fact, does not affect materials but the winding strategy. As already explained, PMSM usually are designed with distributed windings in contrast to high cost concentrated windings mounted on BLDCs. It has to be said that concentrated windings PMSMs are also present, though much less common.
  The result is very profound since not only are copper wires not winded around magnetic expansions but also coils span more than one tooth.
  The result is shown in Figure 1.8: windings associated to different phases overlap each other, forming a smoother passage for the sinusoidal current.

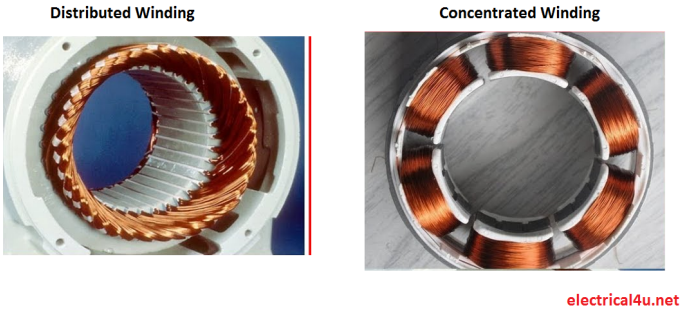

Figure 1.7: Two physical representation of distributed and concentrated windings.

It has to be remarked that the distributed winding solution, despite being the most performing, is, as always, the most expensive and heaviest one. Concentrated winding solution often shows a detrimental effect due to high eddy currents which cancel the benefit of this design choice.

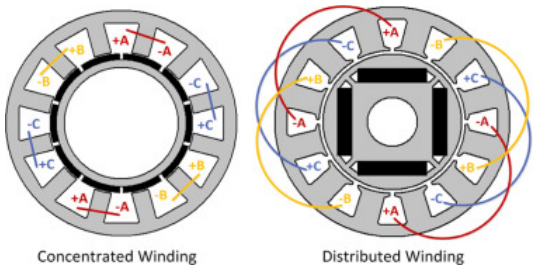

Figure 1.8: Windings scheme for concentrated and distributed solutions.

- **Rotor.** PMSMs rotor technology is, as for the stator, the same of BLDC. Hard and wide hysteresis ferromagnetic materials are implemented since rotors' aim is always to generate a permanent magnetic field which has to be preserved from temperature and the variable magnetic field generated by the stator.
  In PMSM, the rotor magnets are arranged in a slightly different way, since the generated magnetic field has to vary according to the sine of the rotation angle. The detailed description is beyond the scope of this exposition

Working principles and applications

What PMSMs realize is the so-called *Galileo Ferraris* magnetic field (Figure 1.10), that is a magnetic field which rotates in time generated via a three-phase current consisting of three sinusoidal signals 120° out of phase from each other. In fact, the vector sum of the three magnetic field can be modulated in frequency and in amplitude.

The result is a fine control in terms of speed and torque independently, thus enabling the motor to reach any couple of values of torque and angular speed.
The motion principle behind PMSMs is the same as BLDC motors: the stator (*Galileo Ferraris*) rotating magnetic field interacts with the rotor magnetic field

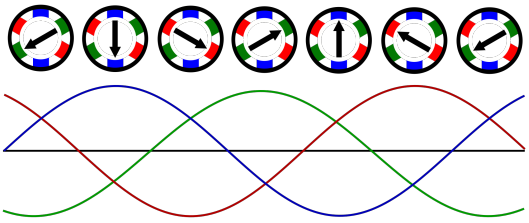

Figure 1.9: *Galileo Ferraris* magnetic field: magnetic field vector (arrow) in function of the three-phase currents.

generated by permanent magnets. The result is a torque which is maximized when the two magnetic fields are shifted by 90°.

One is naturally led to wonder the difference between the AC induction motor (ACIM) and the PMSM, since they are both powered by a rotating three-phase sinusoidal signal.
The first difference lays is the "asynchronicity" of ACIMs. In fact, if PMSM are synchronous (i.e. the two magnetic fields rotate at the same frequency), the rotor magnetic field of ACIMs shows a lag when compared to the stator magnetic field. This is due to the intrinsic working principles of ACIMs: the rotating stator magnetic field has to generate current inside the rotor before the rotor magnetic field is generated from that current itself. As we know, PMSM rotor is already generated via permanent magnets, which were not easy to produce until a few years ago. They however share the absence of any electrical link to the rotor, since none of the two implies the presence of brushes.

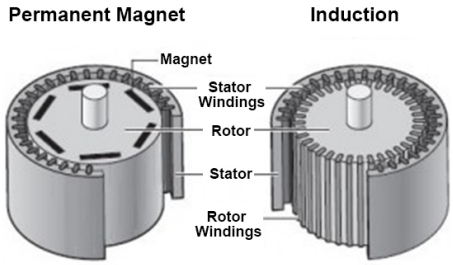

Figure 1.10: PMSM construction and AC Induction motor construction. Notice the lack of windings and the presence of permanent magnets in PMSM's rotor.

Moreover PMSMs need a driver to work while ACIMs just need a sort of frequency control and, in any case, they work better at $60Hz$ with a strong efficiency reduction when compared with PMSM that, on the other hand, are much more expensive.

The conclusion is that PMSM machines show high efficiency, a high power factor, a high torque-to-weight ratio, faster response times. Finally they are fairly easy to control and easy to maintain. On the other hand they are expensive and they need a more precise control.

1.2.3 Final comparison between BLDC motors and PMSMs.

After explaining the main design principles, the most relevant construction method, technologies and materials of the most famous and widespread brushless motors it is necessary to show BLDC motors and PMSM side by side to appreciate differences between the two technologies. A useful table has been proposed by [38]. It sums up the main points we discussed about in a compact and clear way.

BLDC	PMSM
Synchronous machine	Synchronous machine
Fed with direct currents	Fed with sinusoidal currents
Trapezoidal back emf	Sinusoidal back emf
Stator flux position commutation at each 60°	Continuous stator flux position variation
Only two phases ON at the same time	Possible to have three phases ON at the same time
Torque ripple at each commutation	No torque ripple at each commutation
Low order current harmonics in the audible range	Fewer harmonics due to sinusoidal excitation
Core losses due to harmonic content	Less core losses
Less switching losses	High switching losses at the same switching frequency
Control algorithms are relatively simple	Control algorithms are mathematically intensive
Easier to control (six trapezoidal states)	More complex control (continuous three-phase sine wave)
Better for lower speed	Higher maximum achievable speed
Doesn't work with distributed winding	Works with distributed winding
Not as efficient, lower torque	Higher efficiency, higher torque
Low cost	Higher cost
Rectangular current waveforms	Sinusoidal or quasi-sinusoidal current waveforms

Table 1.1: BLDC and PMSM comparison.

Figure 1.11 shows the differences in a very basic control loop: the control strategy, the control signal waveform and the source electric signal.

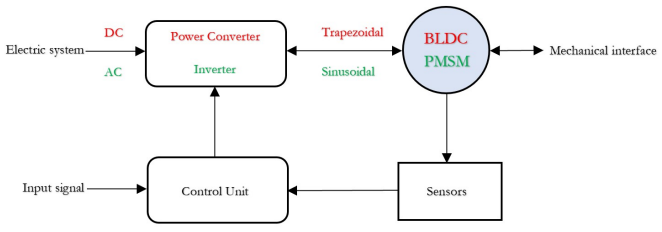

Figure 1.11: BLDC (red) and PMSM (green) basic control loop architecture.

Chapter 2

First test bench

2.1 Test bench description and components.

This first test bench was already assembled and, apart from the external encoder module, it had been designed and constructed with the High Fidelity model clear in mind: to all intents and purposes, it was built around the HF model. In fact, the aim was validating that specific model. Our step forward involves the validation in a more specific condition, that is the presence of mechanical plays at the output gear of the planetary gearbox.
The aforementioned thesis, concerning this test equipment, exploited the internal encoder of the Electrical motor, while our test campaign has demanded an external feedback in order inject mechanical plays and friction and receive the correct feedback in a closed loop.
This bench is made up of an actuation and a breaking module, connected by a chain drive system. Moreover the encoder module is added.
Despite the industrial origin of many parts, their working principles are the same of aerospace components, thus the results and achievements are still valid and absolutely usable. This choice had been made following economic and availability principles.
A view of the bench and a block diagram of the various component are reported in FIgure 2.1 and 2.2 respectively.

The three red dots in the latter scheme symbolize the new encoder adapter, linking the encoder and the gearbox output gear.

2.1.1 Actuation module.

The actuation module is made up of an integrated modular high-performance Siemens motor environment, the *Sinamic S120 AC/AC Trainer Package*. This package provides full authority for the shaft motion, thanks to softwares and web applications, which, through a Microbox PC and the Control Unit, control the inverter and finally the motor. The motor output shaft is linked to the gearbox input shaft through an elastic coupling. Finally the motion is sensed by the external encoder, with the possibility of variable mechanical plays thanks to the encoder motion assembly developed by us.

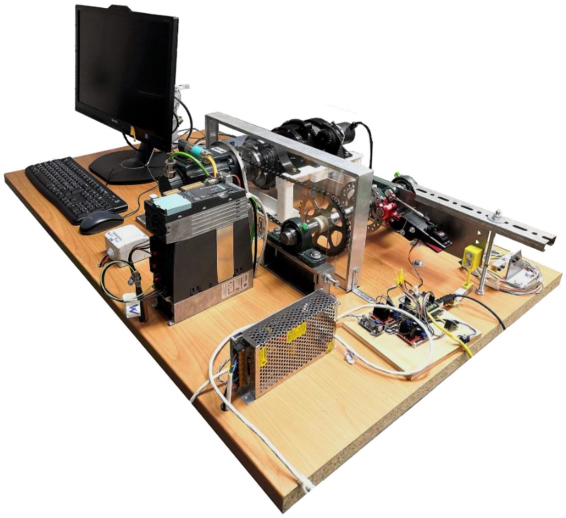

Figure 2.1: The test bench before the external encoder modification.

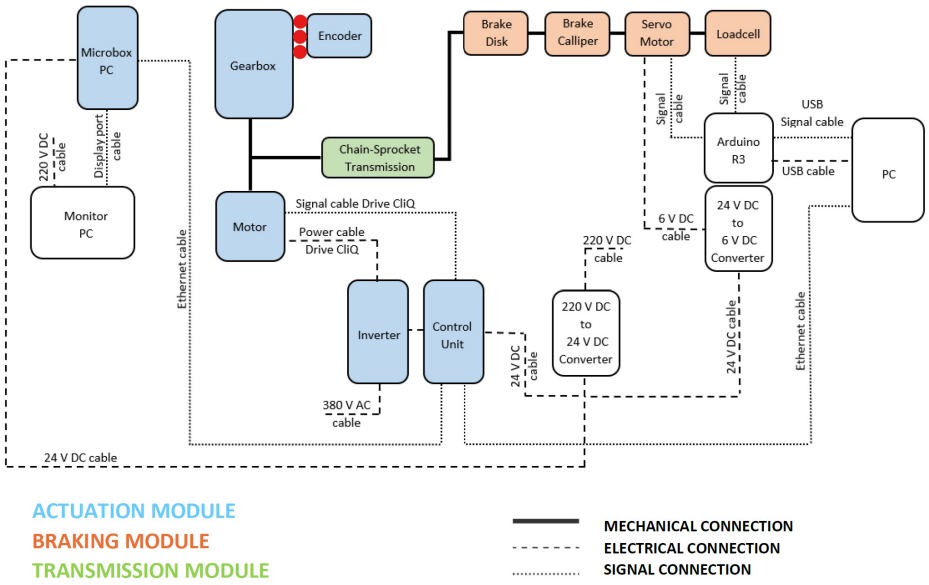

Figure 2.2: Test bench block diagram (as taken from Boschetti master thesis [26]).

Motor

The implemented motor is a Siemens permanent magnet synchronous motor (PMSM): the SIMOTICS S 1FK7060-2AC71-1CG0.
The motor is equipped with the DRIVE CliQ interface with enables fast and easy communication between different components. This PMSM is connected to the gearbox input shaft via an elastic coupling and to the chain via a gear wheel. On the other hand, connections with the control unit and the inverter are obtained with Ethernet cables.
As stated before (Section 1.2.2), PMSM are considered the best solution in terms of

Rated speed (100 K)	2000 rpm
Number of poles	8
Rated torque (100 K)	5.3 Nm
Rated current	3.0 A
Static torque (60 K)	5.00 Nm
Static torque (100 K)	6.0 Nm
Stall current (60 K)	2.55 A
Stall current (100 K)	3.15 A
Moment of inertia	7.700 $kgcm^2$
Efficiency	90.00

Table 2.1: Performance characteristics.

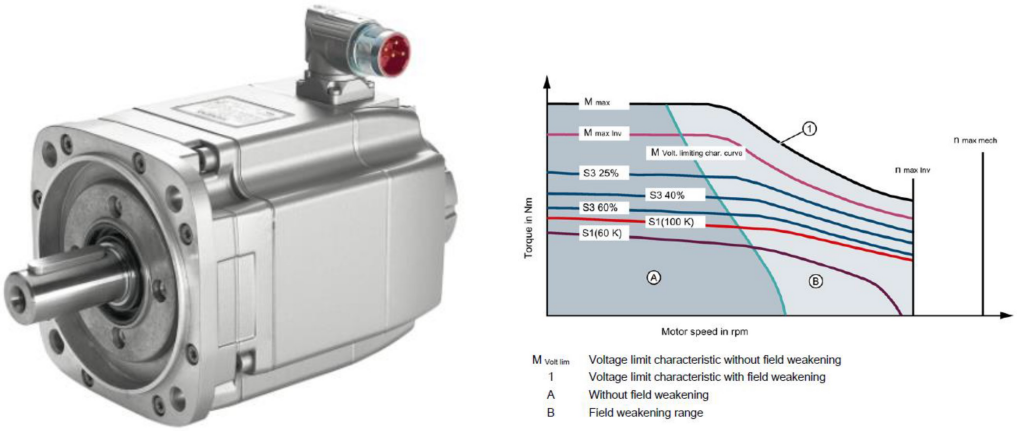

Figure 2.3: Siemens motor and motor characteristics.

torque generation, vibrations, efficiency and power density in the current (and near future) years.
A careful study of the motor dimension and desired placement led to the design and production of the mounting bracket by *Ellena S.P.A*. The bracket supports the motor and firmly fixes it to the table underneath. This "L-like" shape component was assembled with welding points and it is made of a simple steel alloy.

Figure 2.3 shows an image of the selected motor and the graph showing the performance characteristics in terms of torque over angular speed.
The graph is in line with the classical electric motor and shows a decreasing torque due to the increasing value of the BEMF.
In particular, this graph shows: the motor in different working conditions, the different maximum speed and the various regimes limits due to thermal problems for the magnetic materials.
The difference between the continuous and the intermittent area is hence clear. The operating range is, in fact, limited by thermal, mechanical and electronic/electromagnetic issues.

The reported table shows the main engineering characteristics of this motor.

Control Unit and Inverter

In order to provide power and full control capability, the test bench is equipped with a *Blocksize PM240-2* power module (inverter) and a *CU310-2 PN* control unit.
The former, powered by a three-phase 380V AC voltage, placed directly between the control unit and the motor itself, controls the input currents for the correct shaft motion. The latter, mounted on top of the inverter thanks to proprietary mechanical connections (PM-IF), sends signals to the inverter thanks to the internal encoder feedback and the input signal. In this way, the switching of electric signal between the three groups of windings inside the motor case is achieved. As stated before (Section 1.2.2), through a careful tuning of frequency and voltage on each phase, the correct torque and angular speed can be obtained easily, thanks to PMSM internal architecture.
The control unit is connected to the motor via the aforementioned *DRIVE CliQ* interface and to the PLC emulator through an Ethernet connection.
Thanks to well-placed electric terminals, visible on top of the control unit, signals can be exchanged between the unit and an external Arduino board too. This will be useful to synchronise the experimental test data sets. This unit, powered by 24V DC, also provides a port for a flash card, which contains important settings and firmware information.

Figure 2.4: Siemens power module (inverter) and control unit.

Microbox PC and converter

This fan free programmable logic controller allows measuring and control operations. In our application, this PC, designed for maximum performance for complex and demanding control, data collection or communication tasks, is exploited to provide the system with a sinusoidal command, defined in terms of amplitude and phase. The systems exchange data via PLC, which is handled with this PC, connected to the Control Unit through an Ethernet cable, to a monitor through a Display port, and to a keypad-mouse set using USB cables.
Some of its main advantages are:

- fast data processing thanks to high performance DDR4 RAM mounted;
- reliable, fan free rugged and slim design, optimal for industrial environments;
- promised reduced maintenance costs thanks to high system availability.

All these features, which were not fully exploited in our test bench, show how this class of components provide an ideal environment for testing algorithms and control strategy. In other words, despite the low budget, the test bench is an optimal scaled down model of a real industrial application. On the other hand a simple COTS converter is used to get 24V DC from the line voltage of 220V AC.

Figure 2.5: Siemens microbox PC and COTS converter.

Planetary gearbox

The main component of the test bench is the planetary gearbox, entirely designed, built and assembled inside Politecnico di Torino. As will be better explained (Section 3.2), the implementation of a planetary gearbox instead of a traditional ordinary gearbox has a lot of advantages, among which: overall dimensions, absence of offset and misalignment between input and output axes, high transmission ratios, reduced weight and friction etc.

The planetary gearbox has been build using 3D printing Fusion Deposition Modelling techniques in PLA with carbon fibers on some components while the most parts were build using simple black PLA.

Polylactic acid (whose mechanical properties are reported in 2.2) is a world wide best seller for low cost 3D prints thanks to the low cost, low weight and the the simple overall production and design phases.

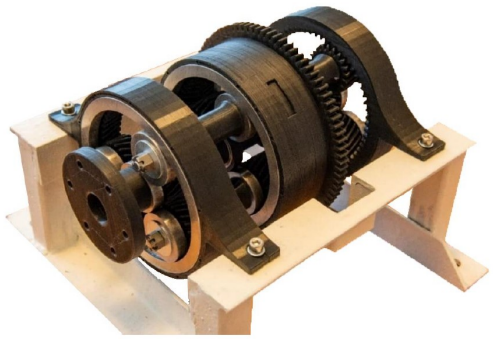

Figure 2.6: PLA planetary gearbox.

Being a vegetable-based plastic material, PLA is usually produced using corn stark or other vegetables raw materials: the result is a fully biodegradable thermoplastic polymer consisting of renewable materials.
PLA has medium mechanical properties but the printing process layer by layer makes structural FEM simulation quite difficult due to the very peculiar overall non homogeneous structure.

Furthermore PLA parts can be glued together with easy accessible solvents and

Properties	Values
Density	1.24 g/cm^3
Tensile strength	60 MPa
Flexural strength	108 MPa
Elongation	9%
Young's modulus	3100 MPa
Shore hardness, *D*	85 Sh D
Melting temperature	145–160 °C
Glass transition temperature	56–64 °C

Table 2.2: PLA typical mechanical properties.

glue; this method has been exploited for the gearbox in various sub-assemblies.
Thanks to the positive features of this affordable and versatile plastic, PLA is typically exploited in first design phases and for prototyping.
Hence the choice of producing the gearbox with this technique: low costs, rapid development, in house troubleshooting, relatively easy design.

The gearbox is connected to the motor output shaft with an elastic coupling, while the output ring is connected to the encoder.
In a generic EMA a gearbox is often an essential component between the actuator and the load.
In fact, usually, high torques and relatively low angular speeds are required. On the other hand, high torque motor are generally big and heavy ones, hence not a viable solution where lightness is an essential requirement.
The solution is exploiting a smaller motor with lower available torque but higher maximum angular speed and then, trough a gearbox, reducing angular speeds while

increasing torque.
It goes without saying that, being gearboxes essential components, they must be considered inside the diagnostic and prognostic model loops: mechanical plays, frictions etc must be examined.

The Planetary gearbox is made up of different shafts, a total of 4: the gears scheme is reported in figure 2.7.

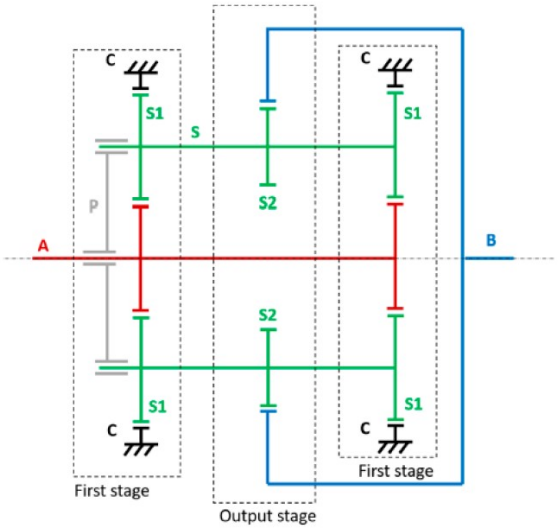

Figure 2.7: Planetary gearbox scheme.

Shaft A (red) and B (blue) are the input shaft and output crown of the gearbox respectively. Shaft A presents a solar gear made up of two wheels, with a total number of teeth z_A, piled up with three spacers. The solar gear determines the rotation of the planetary gears (a total of 3, with number of teeth z_{S1}). The ouput crown (B) is connected with the satellites with a total of z_{S2} teeth.
An interesting design choice has been made concerning the central wheels: in fact they present a specular toothing angle to mount simple bearings withouth the need of a planet carrier, since all shaft are self-supporting.
The detailed gearbox design process is visible on Sciandra and Boschetti thesis ([40], [26]).
The most important formula links V_A, the speed at the input shaft and V_B, the speed at the output shaft.

$$V_B = V_A \frac{r_{S1} - r_{S2}}{2r_{S1}}$$

Where r_{S1} and r_{S2} are the radii of S1 and S2 satellites respectively.
Thanks to element C, the gearbox is firmly fixed to the test bench table trough a steel support.
The gearbox main mechanical data are reported in the table below (Table 2.3) and were obtained in Sciandra and Boschetti thesis with classical Willis formulas:

Planetary Gearbox	
Number of teeth	
Z_A	21
Z_{S1}	21
Z_{S2}	20
Z_C	63
Z_B	62
Degrees of freedom	1
Reduction ratio	124
Total inertia reduced to A	$1.75*10^3$ g mm^2

Table 2.3: Planetary gearbox data.

2.1.2 Breaking and transmission module.

A breaking module is essential to simulate realistic conditions, for instance the presence of external aerodynamic loads on the output shaft. This is achieved trough a breaking torque obtained with a steel disk break system.
Another steel shaft is placed parallel to the gearbox and fixed to the basement with two self-aligning bearing assemblies. A chain links the motor output shaft with the breaking shaft trough a sprocket. A brake disk, with proper holes for heat dissipation purposes, is fixed to the breaking shaft.
The breaking assembly resembles cycling sector brakes. The brake is actuated via a servomotor, similar to the ones used in the model making sector.
In fact, a metal plate is placed between the two bearings: this plate houses the 3D printed connection where both the breaking assembly and the servomotor are fixed. The servomotor output shaft is connected with a steel rod to the brake assembly, consisting of two pads which can make contact with the disk, generating friction, hence transferring an external load thanks to the steel chain.
A load cell is mounted to the metal plate to measure the mechanical deformation during the tests. Thanks to the cell measurements, read by an Arduino board, is possible to calculate the force and the breaking torque.

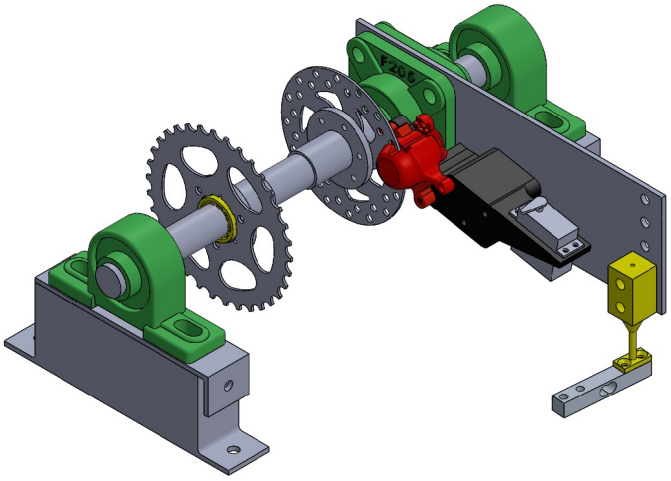

Figure 2.8: Breaking assembly.

Servomotor and its control law

The chosen servo is a digital servomotor (DM5163M) and requires 6V DC. An in-

Figure 2.9: The servo actuator.

teresting insight concerns the code which controls the servo and hence the breaking torque. An Arduino board controls the breaking pads displacements and their generated torque. The control is in closed loop and the breaking connection is controlled with a position command.
Two versions of the software have been developed: one with a potentiometer and another one with the value of breaking force set via Arduino proprietary serial port and monitor.
The *"set"* signal, corresponding to the breaking torque, can be therefore assigned with the potentiometer in the first stage and via the serial port in the final stage of tests; respectively a breaking action is applied. The rough value of total brake force is sensed through a load cell, whose measured value is given as a feedback to the Arduino board which can calculate the error.

$$Error = set - load$$

In fact, the Arduino board disposes of both the set signal and the effective load applied by the breaking system and sensed by the load cell.
The error is then handled via a *PI* controller, which stands for *"Proportional-Integral"*. This special category of controllers, widely used in industrial applications, employs a simple proportional logic with a constant gain and an integral action aimed at reducing the steady state error.
A derivative controller is not used since in this application the error reduction at steady state is much more important than response.

$$Y = y_p + y_i = GP \cdot error + GI \cdot \int errordt$$

After reviewing the control logic, we still have to link the force of the disk brake and the displacement carried of by the servo arm. These analysis steps, carried out by Sciandra and Boschetti ([40, 26]), are reported below and show a great effort with many tests to correlate these two quantities.
The results can be seen in the graph reported in figure 2.10 where, after a great number of tests, an highly non linear relation can be envisioned. An equation which can be used to approximate this curve is:

$$brakeforce = \left[\tanh\left(\frac{angularposition - 115}{35}\right) + 1\right] \cdot 900$$

which, expressed in terms of angular position is:

$$angularposition = \frac{35}{2} \cdot \log\left(\frac{brakeforce}{1800 - brakeforce}\right) + 115$$

This final equation, used as a lookup table, presents a clear relation between the servomotor command and the effective brake force which can be used inside the Arduino script.

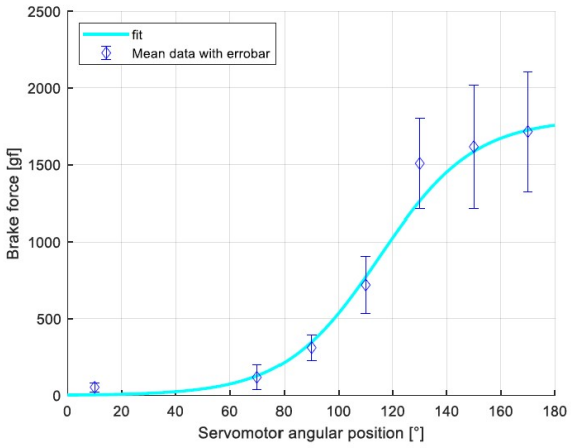

Figure 2.10: Force position feedback.

Transmission: the chain

The chain is used to bind the rotation of the main shaft with the one of the second shaft, connected to the brake disk. In this way, it serves a double purpose: it transfers the motor torque to the brake disk and the brake torque to the motor shaft and the gearbox.
As for the brake assembly, the adopted chain is similar to the ones used in the cycling sector, thanks to the low friction, acceptable noise and the possibility of having the two shaft distant from one another with a low impact on the overall weight. These are the reasons why this system has been chosen. A roller chain is made up of single section repeated along the chain. A single segment is composed of rollers, pins and links (Figure 2.11). In order to work correctly, the chain has to be sufficiently lubricated and tensioned to reduce noise even more.

In our case, the sprockets present the characteristics reported in Table 2.4

As a result the transmission ratio is calculated below. It is the ratio between the number of teeth of the sprocket on the braking shaft and the number of teeth of the sprocket on the motor shaft.

It has to be noted that this transmission ratio enables to exploit the breaking torque at its best. In fact, a transmission ratio not equal to one was purposely chosen and realised with two different sprockets.
The brake can generate around $20 - 30Nm$ of torque; on the other hand the stall torque of the Siemens motor is around $6Nm$. This would have led to the servomotor

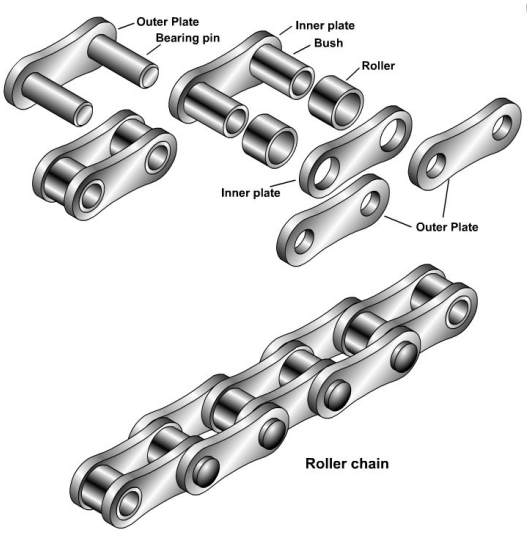

Figure 2.11: Chain elements.

Sprockets	
Motor sprocket	
Diameter	14.2 cm
Teeth number	34
Brake sprocket	
Diameter	9 cm
Teeth number	23

Table 2.4: Chain data.

$$transmission\ ratio = \frac{z_{motor\ sprocket}}{z_{brake\ sprocket}} = \frac{\omega_{brake\ sprocket}}{\omega_{motor\ sprocket}} = \frac{34}{23} = 1.48$$

working well outside its optimal operating range with increased internal frictions, random errors, lower test repeatability etc
Thanks to this transmission ratio the breaking torque felt by the driving shaft (i.e. motor shaft) is lower, therefore the servomotor can work in the best conditions possible.

Figure 2.12: Transmission CAD model.

2.2 Encoder support module.

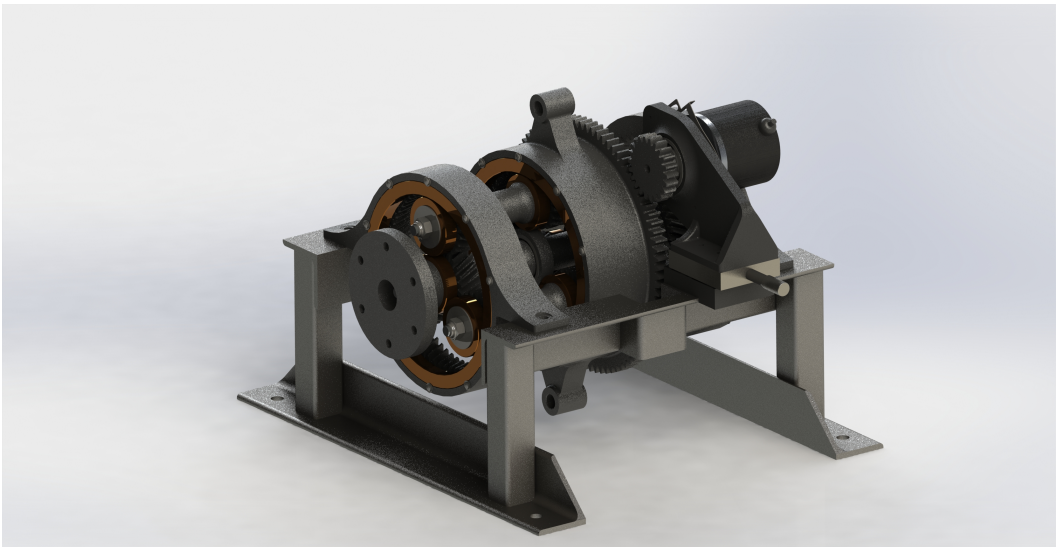

Figure 2.13: Transmission assembly rendering with the newborn support.

One of the first steps has been completed with the design and production (via FDM technique) of the encoder support which was then mounted onto the main gearbox to provide variable mechanical play between the encoder and the external output (user) ring of the transmission. In this way, useful data can be saved by varying the mechanical play to simulate fatigue effects due to components wear in real life applications.
The encoder support assembly is composed by three main components:

- the encoder support itself (central image in Figure 2.14);
- a micro-controle linear translation stage (micrometer) (grey object in Figure 2.14);
- a platform for the micrometer (left image in Figure 2.14).

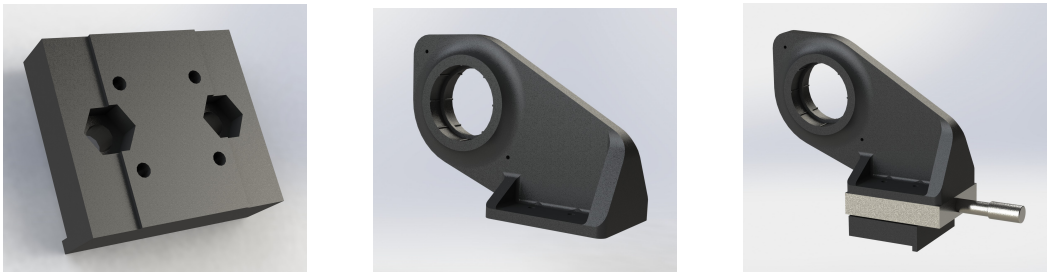

Figure 2.14: Platform, encoder support and assembly with the micrometer.

The three parts are linked together with bolts, washers and nuts as depicted in figure 2.14.

A careful design has been achieved to protect the encoder and the gear attached to it by placing the micro-controle stage in a way that its internal spring does not push the encoder assembly towards the transmission. In fact, by moving the knob it is possible to widen the mechanical play in contrast with the spring force. This is an inherent safety feature since, if any mechanical problem were to happen, the encoder gear could move away from the transmission external ring gear preventing fatal damage to the structure.
The support assembly was modeled in *SolidWorks* environment and then realized with FDM technique in PLA with an infill percentage of 70%. Various ribs are placed to make the support even stiffer; different holes were provided to accomplish a perfect match between the parts with special slots for bolts head. Finally, the holes for ball bearings were created along with the space for the encoder itself.

This small but essential encoder assembly was exploited by eng. Luca Boggio and Dr. eng. Matteo Bertone, who carried out the mechanical tests with different play configurations and different input signals.

2.2.1 Encoder

An encoder is a device that translate angular motion or position of a shaft into an analog or digital signal to identify position or motion.
In our case, the encoder is an incremental, digital, optical encoder. Optical encoders are very common for their low cost, high precision and reliability.
The input shaft is integral with an optical disc, which presents very small holes or slots: on one side of the disk a light source is positioned, while on the other side an optical sensor detects light as it passes through the marked disc. Incremental encoders do not indicate the absolute position, hence they output a "Z" signal which keeps track of the turns. Apart from the "Z" signal, the encoder outputs two other signals: "A" and "B" to keep track of the angular position. According to the sequence of signal and the time between them, the position and speed of the shaft can be determined. The encoder mounted is a TSW581HS by Italsensor, high precision with a pulse rate of 5000.

Figure 2.15: The encoder used in our test bench.

Chapter 3

Second test bench

In the context of this thesis, another experimental test bench has been designed from scratch.
This bench will be useful for fatigue tests on small planetary gearboxes. Once again, the aim is to collect and gather important data about the trends of different parameters while each gearbox is stressed until the breakdown due to fatigue is verified.
The life-cycle of these components is known, in fact this study does not set as its target a gearboxes fatigue study. This test bench is designed to bring each gearbox to its breaking point by applying a much higher torque than the nominal one to break it in a reasonable amount of time. This goal can be achieved via a careful design and sizing of the test bench components which have to provide enough stress to the gearbox to break them but not too quickly.
The testing platform was design according to the following TLRs (Top Level Requirements):

- compact and mobile platform;
- installation and design of reusable components, which might be used in future research projects;
- low cost;
- interface with pre-existing component (e.g. motor inverter and control unit, table etc);
- low friction at the shaft (resulting in a small number of bearings);
- modular design;
- usage of COTS component wherever possible;
- easy to manufacture components.

The result is a compact but powerful test bench with the following features (numbers referring to Figure 3.1):

- different gearboxes to test (1);
- Siemens PMSM (2);

- a platform for the motor, with different bores and holes (3);
- a flywheel to provide inertia to the gearbox output shaft (4);
- two auto-aligning ball-bearings with their supports (5,6);
- an elastic coupling (7);
- a steel link, fixed to the main support, which houses the gearbox (8);
- a steel shaft constrained with two ball bearings (9);
- a steel flange (10);
- an hollow-shaft encoder and its 3D printed support (11);
- a steel link which connects the motor shaft to the gearbox. The end of this component can be seen as the input *sun* of the gearbox itself (12);
- bolts, nuts, washers, keys, Seeger rings etc.

In the next sections each component will be examined in details and their design choices will be explained.
Before reviewing each mechanical piece one by one, it is better to analyze the test bench in general and introduce the key mechanical component: a planetary gearbox.

3.1 General Overview.

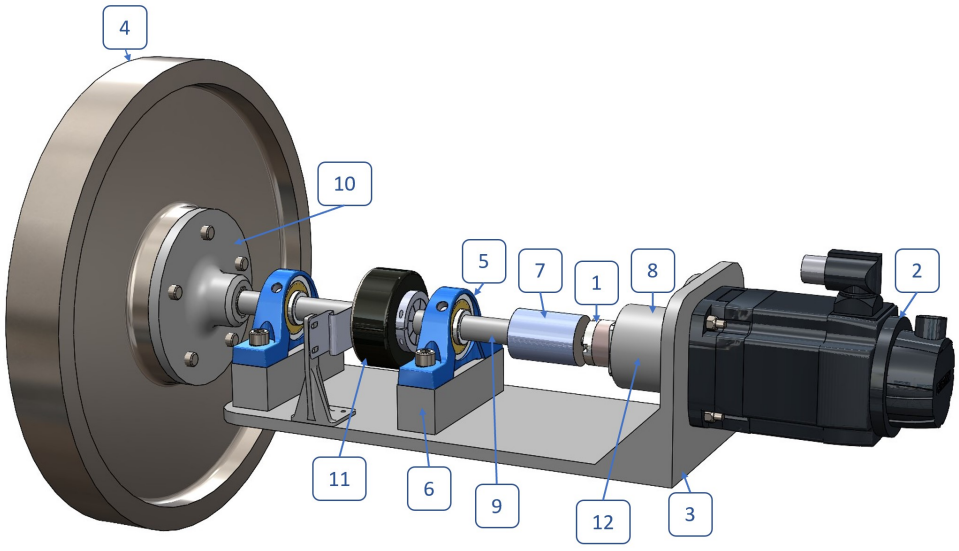

Figure 3.1: General test bench overview.

Figure 3.1 shows the final configuration of the test bench, consisting of 12 main elements.

The motor, fixed on the vertical bracket of the main support, is kept aligned with the main shaft and the other components.
The motor, controlled by the Siemens proprietary software TIA or other web-server applications already exploited in the study for the first test bench, following a sine signal with precise amplitude and frequency (see Section 3.4) causes a back and forth rotation of its output shaft. The shaft is integral with a specially design component, which ends up in a spur gear, this is the input sun of the gearbox as can be seen in figure 3.2.
The gearbox is fixed to the external steel component (i.e. the "cup") (number 8 in figure 3.1), while its output shaft is locked into an elastic coupling which links it to the main shaft. The main shaft ends up with a steel flange, fixed with a key, a Seeger ring and a washer as will be explained later on (Section 3.5.8).
The flywheel in fixed to the flange with five bolts.
The main shaft is sustained by two ball-bearing assemblies, mounted on two precisely designed steel supports.
Finally an encoder, fixed with a 3D printed support, reads the flywheel movements.
Each component is designed with a clear and precise idea in mind; various versions of each component were designed to reach the optimal configuration. In every design process, trade off are essentials and in this, despite simple, design I learned that many requirements are always involved.

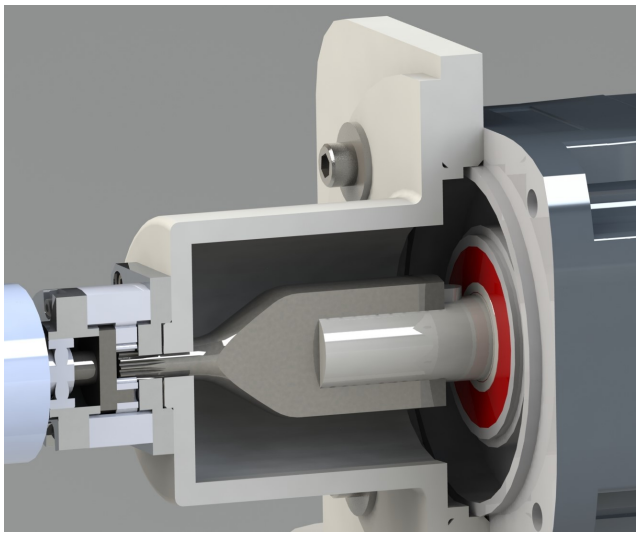

Figure 3.2: Section view of the assembly.

3.2 Planetary gearboxes.

The tested gearboxes exploits a very useful and compact way of exchanging speed and torque from the input shaft to the output shaft: the planetary technology.
A planetary gearbox is essentially a more or less complex system which is characterized by the presence of at least one rotary hub which is revolving about a central *sun gear* or *sun wheel*. The transmission ratio and the number of stages of our gearboxes are reported in the table below. Planetary gears are at the heart of nowadays

Figure 3.3: Adopted planetary gearboxes.

	Gear ratio	**Number of stages**
Gearbox 1	3.71:1	1
Gearbox 2	13.73:1	2
Gearbox 3	50.89:1	3

Table 3.1: Gearbox features

engineering components, even if their mechanical working principles is envisioned since the 15^{th} century by Leonardo da Vinci, who took inspiration from the planets movements. The name *planetary* and all the different parts definitions derive from the analogy with the complex system formed by the sun and the other planets. In fact, inside a planetary (or epicyclic) gearbox we can find different mechanical parts called: *sun gears, sun wheels, planet or satellite gears* but also the carrier, rings etc. A generic planetary gearbox stage is made up of 4 main components (Figure 3.4):

- The sun gear;
- Multiple planet gears;
- A carrier, onto which planet gears are fixed;
- An outer ring.

Where the transmission ratio increases, more than one stage could be needed; more than one set of planets can be mounted too.

Usually, in the so-called *wheel drive* gearboxes, the *sun-gear* is moved as the input shaft, it thus move the *planet carrier*, which makes the *planet gears* rotate, since they are locked in the *planet carrier*. The planet gears engage with the *satellite (or ring) gears* which is the housing. This systems recalls the movement of the fixed sun and the revolving celestial bodies.

In other words, the main input shaft ends with the *sun gear* itself, which is placed at the very center of the gearbox assembly. It transfer the rotation to other

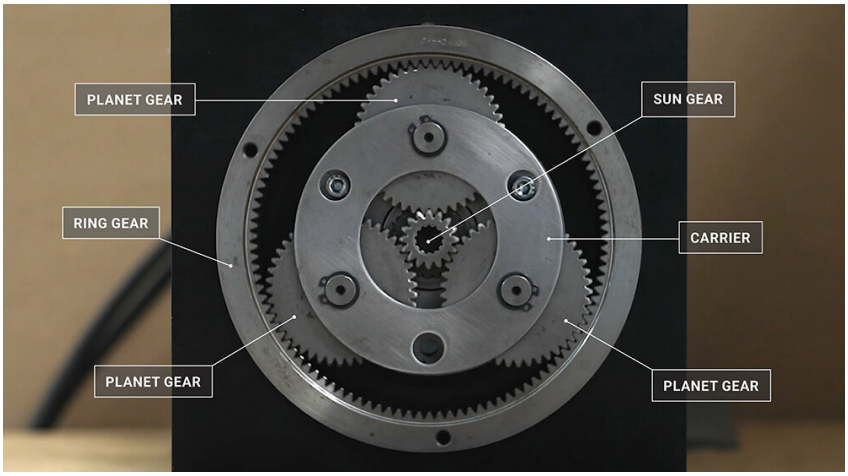

Figure 3.4: A simple planetary gear stage with three planets.

gears called *planet gears* or *satellites*, which are fixed, trough hubs, to the *planet carriers* and rotate inside an internal gear which is the *ring gear* itself.
Unlike celestial movement, a planetary gearbox can drastically change the result of its application by changing the driven input and the controlled output shaft but also the solid part. Hence, a single component can be exploited in very different ways.
Other types of epicyclic gearboxes are called *shaft output* and *spindle output*.
Usually planetary gearboxes are used in the transmission where high torque conversion in small components is needed, given the typical compact size and high torque density these devices provide. Moreover they present high efficiency too.
The gearboxes we adopted are members of *wheel drive* family, in which the sun gear drives the planetary gears, fixed to the carrier.
In these gearboxes the sun presents 17 teeth, the three satellites 14 and the ring gear has 46 teeth.

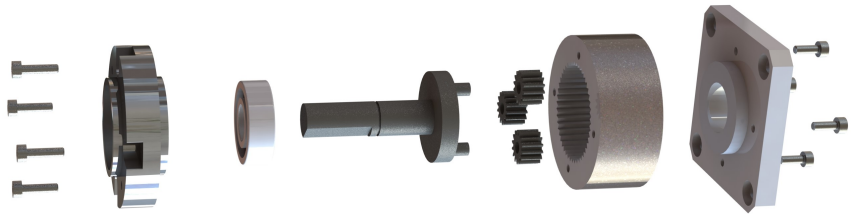

Figure 3.5: Exploded view of the gearbox CAD model.

3.2.1 Gearbox High Fidelity CAD model

To better understand how our set of planetary gearboxes works and to correctly size all the components that are going to interface with them, an high fidelity CAD model of the purchased gearboxes has been developed (Figure 3.5).
This model has been pivotal since the test bench is literally built around the gearboxes.
Given the high importance of this CAD representation, every single component of the gearbox is modelled with high precision.
Every screw is measured and its position was found with a caliber. Also the bearing and the main shaft with the Seeger ring seat is drawn with high fidelity.
The spur gears were created with the *Solidworks* internal toolbox, which made the design of the gears easier with just the need of the external parameters such as the angle of pressure, the diameter, the modulus, thickness and shaft diameter, which are reported in the table below:

Metric Spur gear data	
Modulus	0.5
Number of teeth	17
Pressure angle	20°
Thickness	$5mm$
Shaft diameter	$3mm$

Table 3.2: Metric Spur gear data

The most sensible areas are, of course, the output shaft (diameter and length), the overall dimensions (length) and the interfaces. Finally the gears and their position were essential to correctly size the other component, such as the internal coupler, the external link etc.
An exploded view of the one stage ($\tau = 3.71$) gearbox is shown in Figure 3.5.
A total of three gearboxes models have been developed according to the external dimensions given by the producer and our measurements by hand. In fact, since there are three main sizes of gearboxes, it was important to have a model for each one in order to correctly assess the overall dimension of the test bench. However, since the internal complexity was significantly higher only the first stage one was design in details also internally. The two ($\tau = 3.71^2$) and three-stage ($\tau = 3.71^3$) gearbox are highly representative only for the external features.

3.3 Gear FEM analysis.

To achieve a first set of data in terms of torque and inertia, a simple finite element analysis has been carried out in *Solidworks* environment.
The aim is to determine stresses in the gears with different torque conditions; then the maximum stress value can be compared to the typical yield and ultimate stress values for the gear material and thus the sizing of the motor and the flywheel can be executed accordingly. Also the material's Wholer's curve will be used to assess a reasonable load condition which can leave some margin before the gears' collapse.
Since gearbox information from the seller were quite lacking in terms of mechanical properties as well as in overall load performance, a literature review has been carried out, comparing different gearboxes with similar characteristics.
A steel, commonly used for shaft and gears, turned out frequently in our research: C45 steel (equivalent of AISI 1045). Hence, we assumed this material for the gears. It has to be noted that this assumption is very strong since material mechanical properties play a big role in structural analysis and thermal treatments can deeply change values from the same materials. However we are very confident that the material is similar to the assumed one, since very similar gearboxes exploit this type of steel.
Moreover, this is just a very rough estimation of the torque needed to bring the gears to a collapse and not a design study for the gearbox, so this degree of uncertainty is totally accepted in this phase.

3.3.1 AISI 1045 steel.

AISI 1045 is medium carbon steel widely used in those applications which require medium-high wear-resistance and medium-high strength.
With a tensile strength of $570 - 850 MPa$ and Brinell hardness of around 200, this steel presents good weldability, good impact properties and, more important, very good machinability (for gear manufactoring). These characteristics make this still the optimum compromise in terms of performance and price in applications such as: axles, bolts, rods, studs, gears, axles, shaft and machine parts in general.
This steel can be subjected to different heat treatment: annealing, normalizing, hardening, tempering... The chemical composition for AISI 1045 steel is reported below [4, 2];

Element	Content
Carbon, C	$0.42 - 0.5\%$
Iron, Fe	$98.51 - 98.98\%$
Manganese, Mn	$0.6 - 0.9\%$
Phosphorous, P	$\leq 0.04\%$
Sulfur, S	$\leq 0.05\%$

Table 3.3: Chemical composition of AISI 1045 steel.

Hereafter some physical and mechanical properties used in the analysis are reported [4, 2].

A CAD model for the spur gears was created in analogy with the real part with a

Property	Value
Young modulus $[N/mm^2]$	205000
Poisson coefficient	0.29
Shear Modulus $[N/mm^2]$	80000
Density $[kg/m^3]$	7850
Tensile Strength, Ultimate $[N/mm^2]$	625
Tensile Strength, Yield $[N/mm^2]$	530

Table 3.4: Mechanical properties of AISI 1045 steel

modulus of 0.5 and 14 teeth. (Figure 3.6).
Then the study was set up, imposing constraints, loads and the mesh settings (with

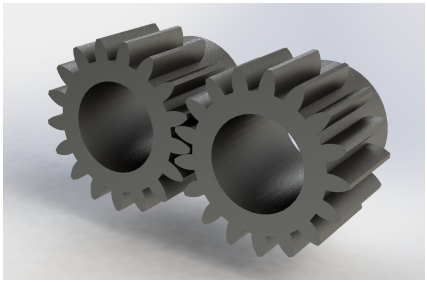

Figure 3.6: CAD assembly for the simulation.

78831 nodes and 50099 elements) (Figure 3.7). Furthermore the mesh is denser near the contact between the teeth. The right gear is totally fixed (both translation and rotation) while the left gear presents a hinge constraint which allows to apply a torque. Hence, the torque is applied on the left gear which pushes against the fixed right gear. In the simulated condition, the contact between the two gear teeth is

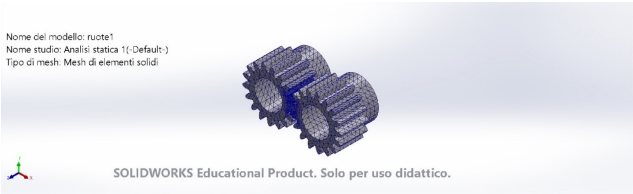

Figure 3.7: Simulation mesh.

located near the tip, this is considered one of the most challenging condition. The stresses were obtained through the *Von Mises* equation.
Different load conditions were simulated, ranging from a torque of $1Nm$ to $20Nm$. The significant results are visible in the next images (Figure 3.8, 3.9, 3.10): in fact, already with a torque of $2Nm$, there are some localized stress higher than the ultimate tensile stress; while already at $1Nm$ of torque yield stress levels are reached.

The results at different torque values are essential for the flywheel design and motor choice.

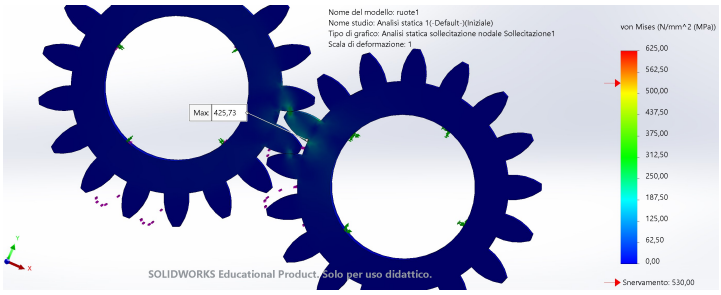

Figure 3.8: Stress levels after $1Nm$ torque.

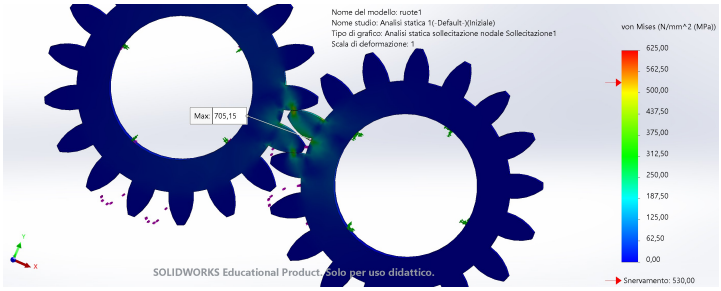

Figure 3.9: Stress levels after $2Nm$ torque.

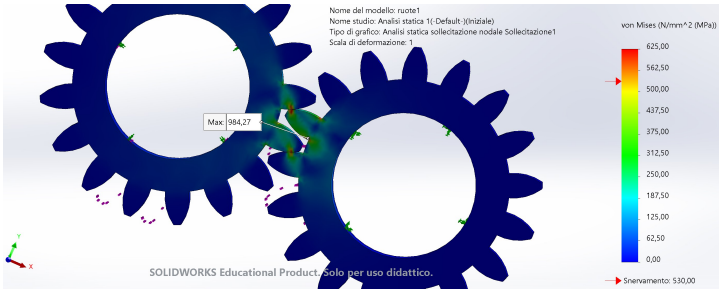

Figure 3.10: Stress levels after $3Nm$ torque.

3.4 Motor and flywheel sizing.

Thanks to a Matlab script I managed to find viable values of many design parameters all at once. In fact, through this multi-parameter and multidisciplinary script both the mechanical parameters, such as the flywheel inertia, the motor RPMs and torque, both the structural fatigue aspects have been taken into account.

Input values were:

- Flywheel inertia J $[kgm^2]$
- Shaft frequency f $[Hz]$
- Motion amplitude A $[rad]$
- Transmission ratio τ

Other essential values were given by the various linear structural simulations in *Solidworks* in order to get the Von Mises σ in the most critical area of the spur gear in different torque conditions (Figure 3.8 to 3.10).
Since the analysis is linear, the relation between torque and structural stresses is a straight line whose coefficient were calculated trough *cftool* in Matlab.
The following table shows the torque applied and the result stress according to *Solidworks* simulations.

Torque applied $[Nm]$	$\sigma[MPa]$
1	425.73
2	705.15
3	984.27
4	1262.4
5	1578
6	1893.6

Table 3.5: Simulation results

The resulting fitting equation is reported below:

$$\sigma = 292.5 \cdot C_m + 117.9$$

where C_m is the torque applied to the gear as in the previous examples in Nm, while σ is the von Mises resulting stress in Mpa. Moreover this linear relation must be limited, introducing a non linearity: a saturation.
In fact, after reaching the ultimate stress value in at least one point, the material would break down. The line is therefore limited at a value of $\sigma_r = 625MPa$, coherent with the selected C45 steel.

Finally, fatigue data are fundamental for this script. Data were taken from [41] where C45 steel is analysed in depth and were an acceptable formulation of the Wholer formula and graph can be found (Figure 3.12).

The result is the following linear regression:

$$\log S_a = -\frac{1}{9.80} \log N + 2.9611$$

where S_a and N are the stress σ and the number of cycles.

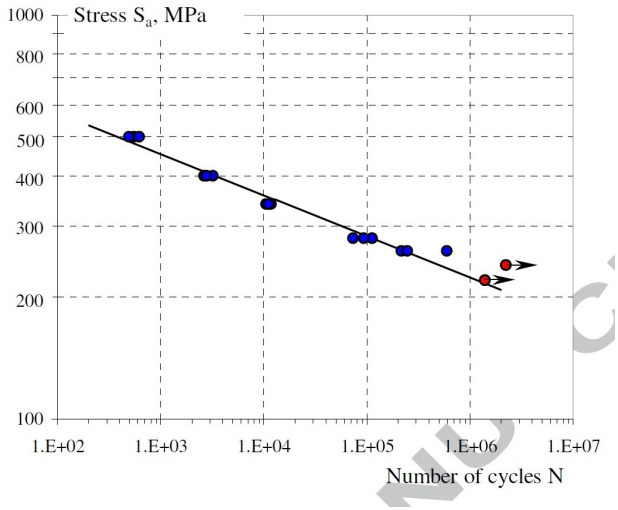

Figure 3.11: Wholer diagram of fatigue life for C45 steel as taken from [41].

The formula, expressed in terms of N becomes:

$$N = 10^{[Log(S_a) - 2{,}9611] \cdot (-9.8)}$$

Figure 3.12 and the associated formulas are consistent with typical fatigue diagrams of aerospace and steel alloys. The Wholer diagram, in fact, shows a decreasing stress value with increasing number of cycles. This means that, on the one hand, the higher the number of cycles, the lower the stress needed to break the component and, on the other hand, that with a specific stress value $\overline{\sigma}$, only $\overline{N}$ cycle can be considered viable. After that value $\overline{N}$, with that specific sigma value $\overline{\sigma}$, the component will break under the propagation of cracks. Finally, it is typical of steel to present a fatigue limit: after reaching very low values of stress, the result is invariant from the number of cycles. In other words, the relation becomes a straight horizontal line, meaning that even much bigger number of cycles with an applied stress lower than the fatigue limit would not break the component.
It has to be recalled that our analysis shall aim at just a preliminary "order of measure" values, hence these fine and detailed considerations can be overlooked.

The script has been tuned for all transmission ratio of the available gearboxes. However, as expected, the most difficult gearbox to break is the one with the lower τ, since there is just one stage (hence the probability of breaking a gear tooth is lower) but, more importantly, the torque ratio is lower and the first (and only) stage gears must endure lower inertial loads at each motion direction reversal.

3.4.1 Matlab workflow

The followed workflow is now discussed in details.

1. **Input parameters initialization.** A reasonable value of inertia for a flywheel is selected, just for a first run (around $J = 0.5 kgm^2$). Moreover, some

values for frequency (around $f = 0.5Hz$), rotation amplitude ($A = 720°$) and the transmission ratio value $\tau = 3.71$, with reference to the first stage gearbox are inserted too.

2. **Kinetics and torque computation.** Now, considering the rotation of the flywheel with the pulsation $\omega = 2\pi \cdot f$, maximum speed and acceleration of the flywheel can be obtained. In fact, starting from the equation

$$\theta = A \cdot \sin \omega \cdot t$$

$\dot{\theta}$ and $\ddot{\theta}$ can be derived. Their maximum value is when the armonic function $cos()$ or $sin()$ is equal to 1, hence:

$$\dot{\theta_{max}} = A \cdot \omega$$

and

$$\ddot{\theta_{max}} = A \cdot \omega^2$$

Maximum torque on the output shaft (the one integral with the flywheel) can be easily obtained, knowing the flywheel (speculated) inertia and the maximum acceleration:

$$C_{max} = J \cdot \ddot{\theta_{max}}$$

Hence the torque on the input shaft (motor) is:

$$C_{m_{max}} = \frac{C_{max}}{\tau}$$

A more reasonable value is the RMS (Root Mean Square) values of torque, hence:

$$C_m = \frac{C_{m_{max}}}{\sqrt{2}}$$

3. **Estimation of stress levels from torque value.** Thanks to the aforementioned *Solidworks* structural analyses Figure 3.8 to 3.10), a well-defined relation which estimates stress values given torque values is obtained.
The relation is reported:

$$\sigma = 292.5 \cdot C_m + 117.9$$

4. **Estimation of the number of cycles.** Wholer experimental relation gives us everything we need to estimate the cycles:

$$N = 10^{[Log(S_a) - 2{,}9611] \cdot (-9.8)}$$

If the number of cycles is higher than $1.1 \cdot 10^6$ the relation is not valid anymore. In fact, when exploiting models or experimental relationships, the range of legit application must be kept into consideration as values outside that range are not reliable.
On the other hand, it is plausible that after many cycles a sort of fatigue limit comes into play.

5. **Post processing.** The number of stimuli to which each tooth in subjected at each second can be obtained as shown:

$$f_{soll} = \frac{(\omega \cdot \tau - \omega) * 3}{2\pi}$$

In fact, there are three satellites for each stage; moreover the frequency is directly proportional to the difference of angular speeds between the omega referred to the motor shaft and the omega of the output shaft.
The time before the envisaged break down of one or more tooth can be expressed (in minutes) as:

$$t = \frac{N}{f_{soll} \cdot 60}$$

To sum up everything that has been stated so far, the workflow can be outlined with the following flowchart:

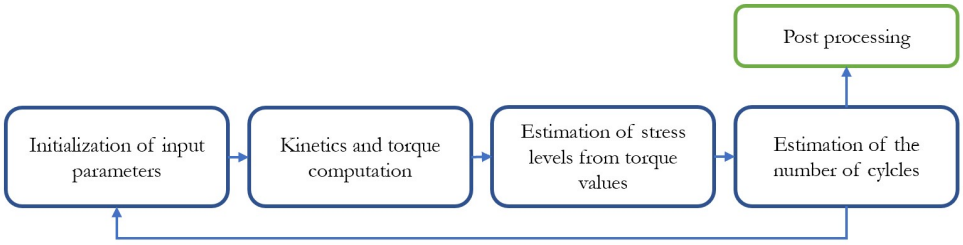

Figure 3.12: Iterative flowchart.

The flowchart explains the iterative nature of this analysis: in fact, only trough different data sets submitted in the initialization phase, it has been possible to reach good values of time before the gearbox breaking, maximum motor speed, flywheel inertia...

This method gave the results shown in Table 3.6, with a $0.5kgm^2$ fixed flywheel inertia. As expected with a fixed inertia of around $0.5kgm^2$ (there is only one flywheel), in order to break down all gearboxes, a motor with at least a torque of $2Nm$ and a maximum speed of around $1500rpm$ is required.

However it must be said that these are only qualitative estimation to guess the size of the motor. In fact, since the input parameters are software-based (i.e. they are not something that cannot be changed during operation), this rough measurement is enough to choose the motor for the test bench.
In other terms, amplitude, speed, frequency of rotation can be changed on the go when the bench is already assembled, without the risk of having an undersized or an excessively oversized motor on the test bench.
For instance, the flywheel inertia has been reduced to around $0.4kgm^2$ in the following design stages in order to meet weight requirements. This change, however, does not invalidate the analysis since, the effect will be a small increase in the rotation amplitudes and transmitted torque or a small increase in breaking time.

In conclusion this simple but useful script has been exploited to understand the general sizing of component, such as the motor and the flywheel, the time to break the gearboxes and the reached stress levels of the gearbox spur gears.
Therefore, this script helped in meeting the most important requirements: sizing a motor and the flywheel aimed at breaking the gearboxes (i.e. they must be oversized for the gearbox) but not at the first rotation, since what we want is to log the trends during the operation (i.e. not excessively oversized). Without exploiting both structural and mechanics theory in a multidisciplinary way this could not have been possible, underlining once more the importance of the integration between different subjects.

$\tau = 3.71; f = 0.25\ Hz; ampiezza = 180°$

Cmotor_RMS	$0.739\ Nm$
Omega_motor_RMS	$5.83\ rad/s\ (55.65\ rpm)$
t	$159\ min$
Sigma raggiunta	$334\ Mpa$

$\tau = 3.71; f = 0.3\ Hz; ampiezza = 180°$

Cmotor_RMS	$1.064\ Nm$
Omega_motor_RMS	$6.99\ rad/s\ (66.78\ rpm)$
t	$12\ min$
Sigma raggiunta	$429\ Mpa$

$\tau = 13.76; f = 0.4\ Hz; ampiezza = 180°$

Cmotor_RMS	$0.509\ Nm$
Omega_motor_RMS	$34.59\ rad/s\ (331\ rpm)$
t	$189\ min$
Sigma raggiunta	$267Mpa$

$\tau = 13.76; f = 0.5\ Hz; ampiezza = 180°$

Cmotor_RMS	$0.797\ Nm$
Omega_motor_RMS	$43.24\ rad/s\ (413\ rpm)$
t	$10.3\ min$
Sigma raggiunta	$351\ Mpa$

$\tau = 51; f = 0.45\ Hz; ampiezza = 360°$

Cmotor_RMS	$0.429\ Nm$
Omega_motor_RMS	$161\ rad/s\ (1532\ rpm)$
t	$95\ min$
Sigma raggiunta	$244\ Mpa$

$\tau = 51; f = 0.45\ Hz; ampiezza = 720°$

Cmotor_RMS	$0.696\ Nm$
Omega_motor_RMS	$145\ rad/s\ (1370\ rpm)$
t	$6.9\ min$
Sigma raggiunta	$321\ Mpa$

Table 3.6: Script results for a fixed flywheel inertia of $0.5kgm^2$.

3.4.2 Matlab script

The Matlab script is here reported with useful comments on its working principles, divided in the following sections (in line with the theoretical dissertation reported before):

1. Flywheel Inertia;
2. Frequency, amplitude, tau;
3. Displacement, speed and acceleration when sin or cos = 1;
4. Torque
5. Sigma with straight line;
6. Compute number of cycles with Wholer;
7. Wholer validity field control;
8. Number of stress for each second for each tooth;
9. Printing results.

```
clc
clear all
close all


% 1. Flywheel Inertia
J =  0.3; % [kg m^2]


% 2. Frequency, amplitude, tau
freq = 0.45; % [1/s]
amp = 720.*pi/180; % [rad]
tau = 3.71; % one stage gearbox
OmegaOut = 2*pi.*freq; % [rad/s]


% 3. Displacement, speed and acceleration when sin or cos =
    1
theta_max = amp; % [rad]
thetadot_max  = amp.*OmegaOut; % [rad/s]
thetadotdot_max = amp.*OmegaOut.^2; % [rad/s^2]


% 4. Torque
C = J .* thetadotdot_max; % [N m]
Cm = C ./ tau; % [N m] Torque and the motor shaft
Cm = Cm./sqrt(2); % [N m] Torque RMS
```

```
27
28
29 % 5. Sigma with straight line
30 sigmavett = [425.73, 705.15, 984.27 1262.4 1578 1893.6];
31 coppievett = [1, 2, 3, 4, 5, 6];
32
33 sigmar = 625; % [Mpa] Ultimate
34 sigma = 292.5 .* Cm + 117.9; % [Mpa] from cftool, linear
       analysis
35
36
37 % 6. Compute number of cycle with Wholer
38 cicli = 10.^((log10(sigma)-2.9611).*(-9.8)); % Wholer
       equation for steel C45
39
40
41 % 7. Wholer validity field control
42 if (cicli >1.1e6)
43     warning("Outside of the range with the submitted wholer
           curve!")
44 end
45
46 Omega = OmegaOut.*tau % [rad/s] Omega all'albero motore
47 Omegacarrier = OmegaOut; % [rad/s] Omega portatreno
48
49
50 % 8. Number of stress for each second for each tooth
51 fsoll = (Omega - Omegacarrier)*3/(2*pi); % [1/s]
52
53 t = cicli./fsoll./60; % [min] Time before break down
54
55
56 % 9. Printing results
57 fprintf('Con J = %.2f kgm2, freq = %.2f Hz, amp = %.2f rad
       (%.2f deg):\n\n', J, freq, amp, amp*180/pi);
58
59 fprintf('Cmotor_RMS = \t\t%f Nm\nOmega_motor_RMS = \t%f rad/
       s (%f rpm)\nt = \t\t\t%f min\nsigma = \t\t\t%f Mpa\n',
       Cm, Omega, Omega*30/pi, t, sigma);
60
61 if (sigma >= sigmar)
62     warning("Teeth are subjected to stress higher than the
           steell ultimate stress (%.1f Mpa)!", sigmar)
63 end
64
65 t = t/60; %[h]
```

3.5 Bench components.

3.5.1 Siemens 1FK7042-2AC71-1CA0 PMSM.

The selected motor is a Siemens PMSM; this decision has been taken to exploit the main components already purchased for the other test bench. In fact, since the series of motor doesn't change, the control architecture does not undergo major changes and the control unit, the inverter and the microbox PC can be interchanged without problems. Finally we wanted to exploit the knowledge we gained working on the other test bench and we wanted to benefit from the control architecture and laws that were already developed.
As stated in the introduction, (Section 1.2.2) Permanent Magnet Sinchronous Motors represent the state of the art of electro-mechanical actuators and they fit well in the current new developed technologies. PMSM, with their high power density, low torque ripples and compactness are used both in aerospace application and in less demanding industrial ones.
The chosen motor is a *1FK7042-2AC71-1CA0* and its main characteristics are reported below:

Engineering data	
Rated speed (100 K)	2000 rpm
Number of poles	8
Rated torque (100 K)	2.8 Nm
Rated current	1.6 A
Static torque (60 K)	2.50 Nm
Static torque (100 K)	3.0 Nm
Stall current (60 K)	1.30 A
Stall current (100 K)	1.61 A
Moment of inertia	2.900 kgcm²
Efficiency	88.0 %

Physical constants	
Torque constant	1.86 Nm/A
Voltage constant at 20° C	122.0 V/1000*min⁻¹
Winding resistance at 20° C	8.60 Ω
Rotating field inductance	64.0 mH
Electrical time constant	7.40 ms
Mechanical time constant	2.15 ms
Thermal time constant	30 min
Shaft torsional stiffness	15500 Nm/rad
Net weight of the motor	4.6 kg

Mechanical data	
Motor type	Permanent-magnet synchronous motor
Motor type	Compact
Shaft height	48
Cooling	Natural cooling
Radial runout tolerance	0.040 mm
Concentricity tolerance	0.08 mm
Axial runout tolerance	0.08 mm
Vibration severity grade	Grade A
Connector size	1
Degree of protection	IP64
Design acc. to Code I	IM B5 (IM V1, IM V3)
Temperature monitoring	Pt1000 temperature sensor
Electrical connectors	Connectors for signals and power rotatable
Color of the housing	Standard (Anthracite RAL 7016)
Holding brake	without holding brake
Shaft extension	Plain shaft
Encoder system	Encoder AM24DQI: absolute encoder 24 bits (resolution 16777216, encoder-internal 2048 S/R) + 12 bits multi-turn (traversing range 4096 revolutions)

Table 3.7: Motor main characteristics (1).

Optimum operating point	
Optimum speed	2000 rpm
Optimum power	0.6 kW

Limiting data	
Max. permissible speed (mech.)	9000 rpm
Max. permissible speed (inverter)	4750 rpm
Maximum torque	10.5 Nm
Maximum current	5.6 A

Recommended Motor Module	
Rated inverter current	3 A
Maximum inverter current	9 A
Maximum torque	10.50 Nm

Table 3.8: Motor main characteristics (2).

From these data, the reasons that led us choose this motor are clear:

- $2.8Nm$ rated torque, optimal for our test where a big amount of torque is needed but without over stressing excessively the gears teeth;
- $2000rpm$ rated speed, ideal for our test campaign;
- Limiting data well outside our required values;
- $2.9kgcm^2$ of inertia, low enough not to invalidate the flywheel inertia calulation;
- Internal 24 bit encoder system;
- possibility of working for extended periods of time.

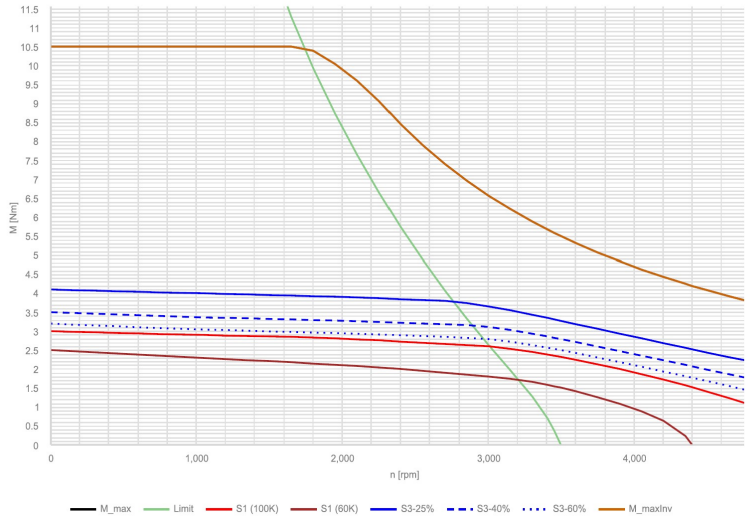

Figure 3.13: Motor main characteristics.

Finally, the Torque angular speed trend is reported (Figure 3.21).
Unlike the first Siemens motor for the other test bench, this one, apart from all

technical characteristics presents a key-seat and a *DIN 6885 6X6X32* key to firmly lock the motor shaft to other mechanical components.
The next figure shows the motor technical drawings, which were essential to correctly size the other mechanical component.

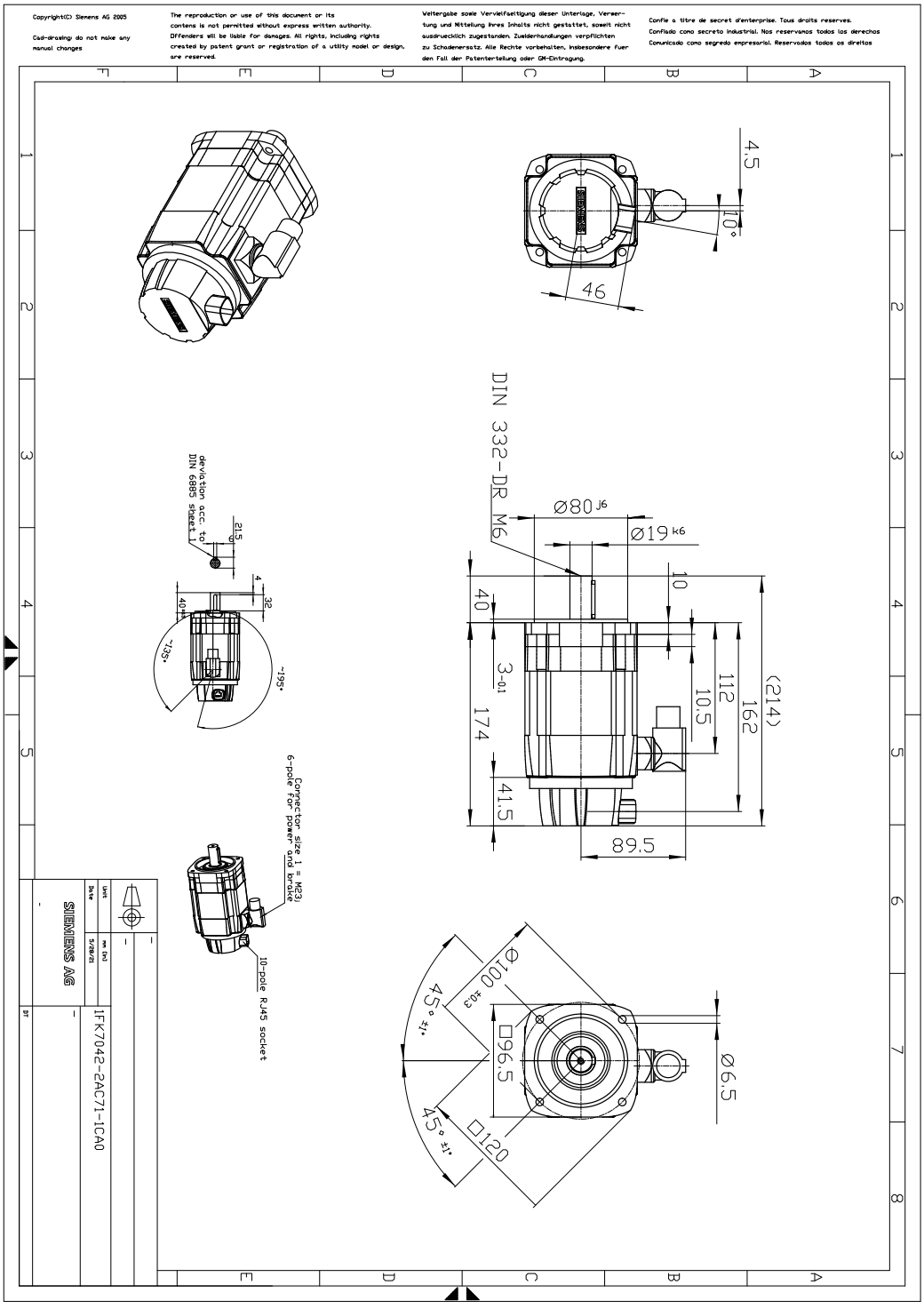

3.5.2 Motor and bench support (Main support).

After reviewing the motor and the general aspects of the test bench, one of the main components is reviewed in more details: the Motor support. It provides the following functions:

- It links all the important mechanical components together on a stable and fixed platform;
- It helps in the strict alignments between the main shaft, the flywheel, the gearbox and the motor shaft;
- It provides an ideal support for the motor trough a bracket with four bolts;
- It can be easily fixed to a table to secure the test bench in place.

The final version of this component presents a big steel plate, 10 mm thick, with different holes: 4 holes for the auto-aligning ball-bearings, 2 holes for the encoder support, one bigger bore for the motor, 4 other circular holes for securing in place the motor and the mechanical link which houses the gearbox. This last version features a long steel plate to make the mounting process easier and quicker, while the motor is cantilevering on the other side.

The first version of the support featured just the vertical mounting site for the motor and 4 holes to fix the base to a bigger platform (See appendix A).

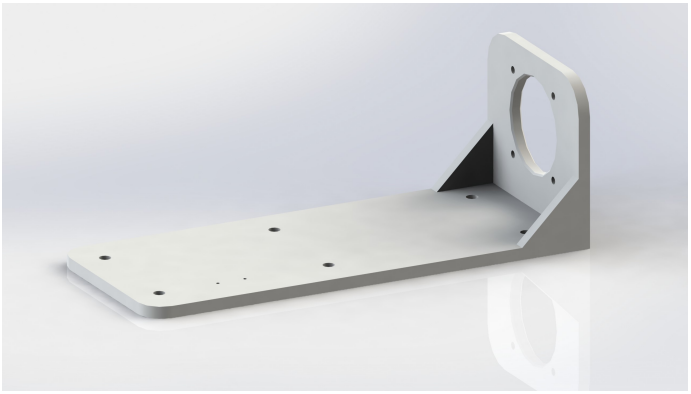

Figure 3.14: Motor and bench support rendering.

The component is designed to be assembled with welding points starting from a metal plate of 10mm. Special tolerances are selected for the flatness of the plate, the perpendicularity between plates, and bores position tolerances. Two reference datums are places on the back of the horizontal plate (to fix the plate to the table) and on the vertical surface (where the motor will be attached). The third reference feature is the center of the main hole for the motor; in this way the position of the plate in the 3-dimensional space is determined. Other dimensional tolerances are present on the motor mounting holes, according to the motor two-dimensional drawings. Finally, another dimensional tolerance is placed on the main hole (80mm) in order to let the motor engage with the support correctly. Chamfers are placed on the inside edges and fillets are placed on the external edges. The 2D drawing is reported in the next page.

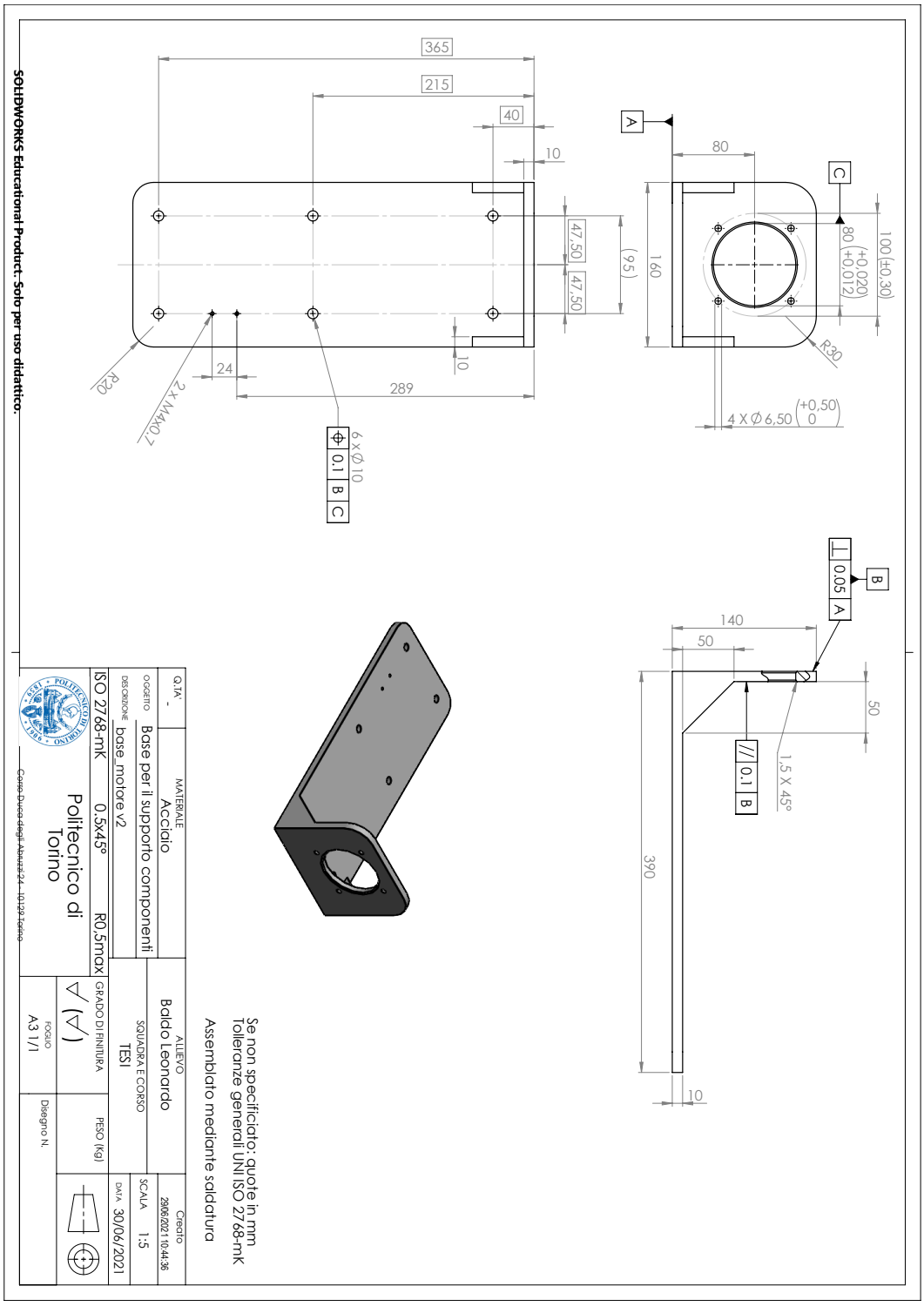
365
215
40
10
47,50
47,50
(95)
24
289
10
R20
2 X M4x0,7
6 X Ø 10
0.1 B C
A
80
C
160
80 (+0,020 +0,012)
100 (±0,30)
R30
4 X Ø 6,50 (+0,50 0)
B
0.05 A
140
50
50
0.1 B
1,5 X 45°
390
10
Se non specificato: quote in mm
Tolleranze generali UNI ISO 2768-mK
Assemblato mediante saldatura
SOLIDWORKS Educational Product. Solo per uso didattico.
Q.TA'
-
MATERIALE
Acciaio
OGGETTO
Base per il supporto componenti
DESCRIZIONE
base_motore v2
ISO 2768-mK
0.5x45°
R0,5max
ALLIEVO
Baldo Leonardo
SQUADRA E CORSO
TESI
GRADO DI FINITURA
PESO (Kg)
Creato
2906/2021 10:44:36
SCALA
1:5
DATA
30/06/2021
FOGLIO
A3 1/1
Disegno N.
Politecnico di Torino
Corso Duca degli Abruzzi 24 - 10129 Torino

3.5.3 Flywheel design.

The flywheel is another essential part for the test bench. In fact, it provides the inertial load which stresses the gears' teeth. The motor shaft, connected to the gearbox sun, continues to rotate back and forth while the output shaft is integral with the flywheel which stands against its rotation.
As already explained in the previous chapters, its sizing has been carried out with a Matlab script and the output of that analysis is now a requirement of a moment of inertia of around $0.4 - 0.5 kgm^2$.
According to classical mechanical design guidelines, the chosen material ins a generic carbon steel, with an assumed density of $0.8 kg/m^3$.
The result is a flywheel with a classical shape with some special features:

- $400mm$ external diameter;
- five $12.5mm$ holes on a $112mm$ circumference. They can be exploited if the flywheel will need some adjustements; in fact, in this way, the flywheel can be mounted onto automotive wheels balancing machines;
- chamfers on the inside of the main bore;
- fillets on the external edges.

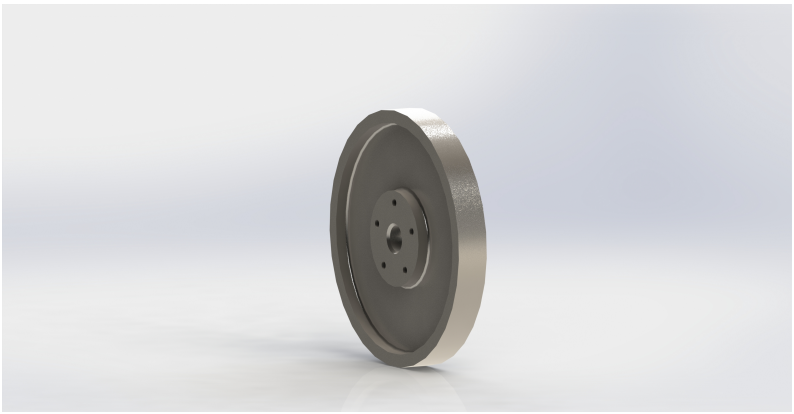

Figure 3.15: Flywheel rendering.

Additional geometric and dimensional tolerances are added: position tolerances for the 5 mounting bores, a perpendicularity and a parallelism. Finally, a circular runout tolerance on the external surface is placed to further limit imperfections.
An H6 bore tolerance is planned to correctly match with the flange with a slight mechanical play.
Through many iteration steps I managed to create a flywheel architecture with a compact size an a mass of around $22kg$ compatible with the stated requirements.
Careful attention was placed in designing the connection, which will be examined later on, between the shaft, the flange and the flywheel. Some mechanical test should be carried out before the main test: for instance some checks concerning the moment of inertia.
The 2D drawing is reported in the next page.

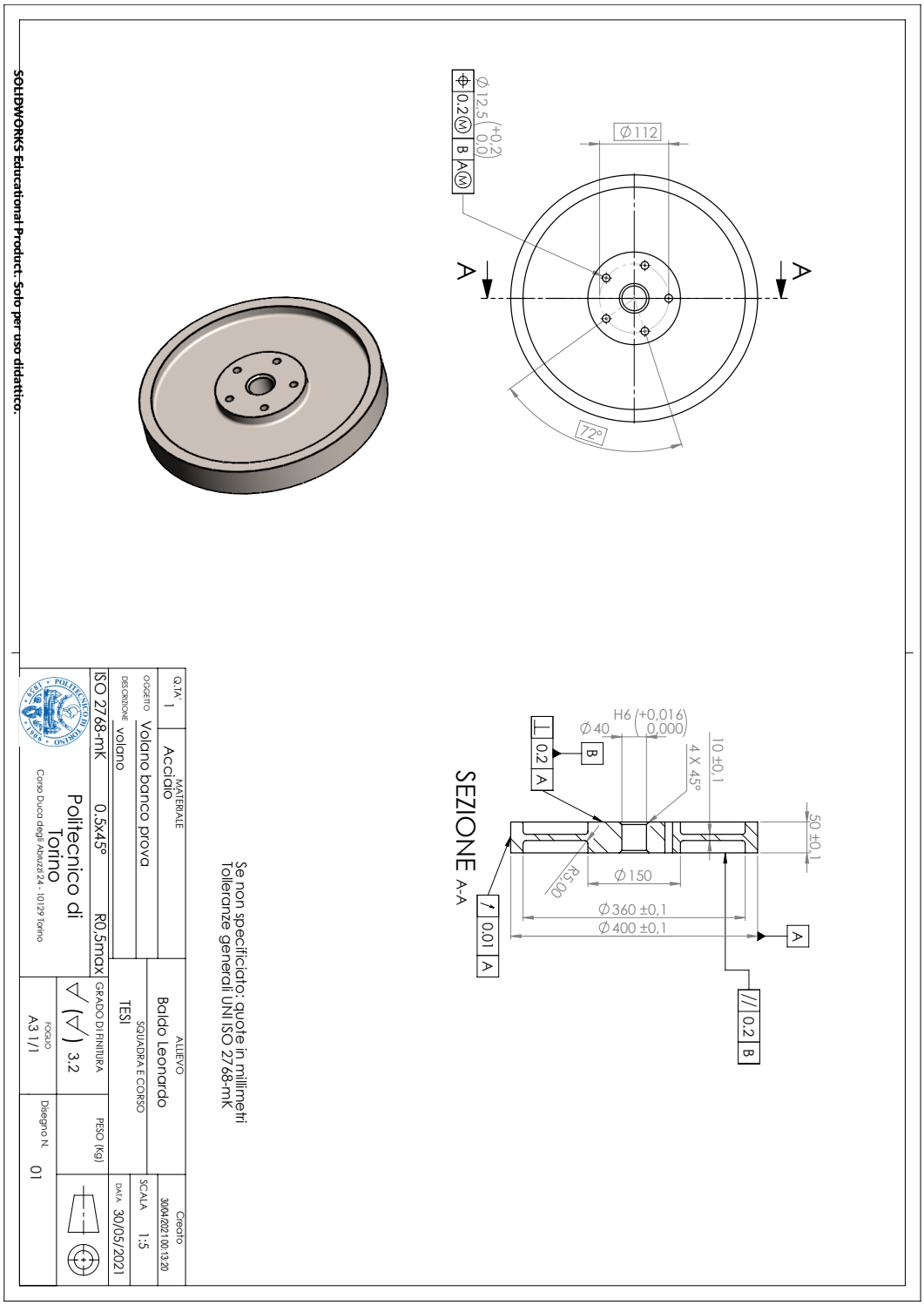
Ø 112
Ø 12,5 (+0,2 0,0)
0.2 M B A M
A
A
72°
SEZIONE A-A
H6 (+0,016 0,000)
Ø 40
B
0.2 A
10 ±0,1
4 X 45°
50 ±0,1
R5,00
Ø 150
Ø 360 ±0,1
Ø 400 ±0,1
0.01 A
A
// 0.2 B
Se non specificato: quote in millimetri
Tolleranze generali UNI ISO 2768-mK
SOLIDWORKS Educational Product. Solo per uso didattico.
Q.TA' 1
MATERIALE Acciaio
OGGETTO Volano banco prova
DESCRIZIONE volano
ISO 2768-mK 0,5x45° R0,5max
GRADO DI FINITURA ▽ (▽) 3.2
ALLIEVO Baldo Leonardo
SQUADRA E CORSO TESI
PESO (Kg)
Creato 30/04/2021 00:13:20
SCALA 1:5
DATA 30/05/2021
Politecnico di Torino
Corso Duca degli Abruzzi 24 - 10129 Torino
FOGLIO A3 1/1
Disegno N. 01

3.5.4 Ball bearings and their supports.

Two USPE 204 ball bearings support from SNR are used in the test bench to sustain the main shaft. These are low friction auto-aligning bearing with cast iron supports. We chose this kind of shaft supports given the specific application we have to fulfill: very low friction (especially viscous), cost-effectiveness requirements and the possibility of fastening the shaft with two grub screws for each ball bearing.
In fact, since the different gearboxes are made up with a different number of stages according to their reduction ratio, there is the need to provide the test bench with the possibility of housing gearboxes with different lengths.
The idea we have come up to is, when it is time to change the gearboxes, loosening the 4 grub screws and letting the shaft shift a in order to house gearboxes with different lengths. This solution, even if not the most professional one, since it introduces a bit of inconstancy between different tests, is the most cost effective one.

Figure 3.16: SNR bearing.

From the bearing support 2D and 3D drawing a support holder to be manufactured in steel is designed. It is just a simple mechanical piece which helps bringing the main shaft at the same height of the motor output shaft.
The result is a steel block with parallelism and perpendicularity tolerances. The wheel base between the two central holes is taken from the bearing support 2D drawing, reported in figure 3.21 along with other interesting values and characteristics.

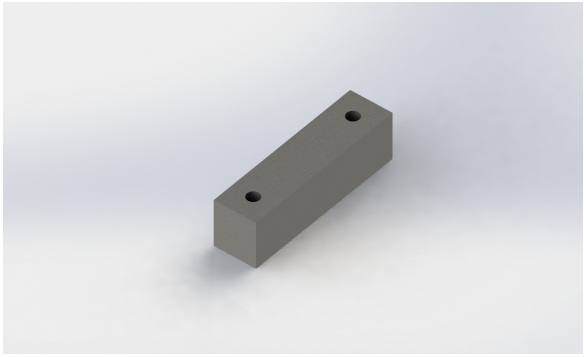

Figure 3.17: Steel bearing support holder.

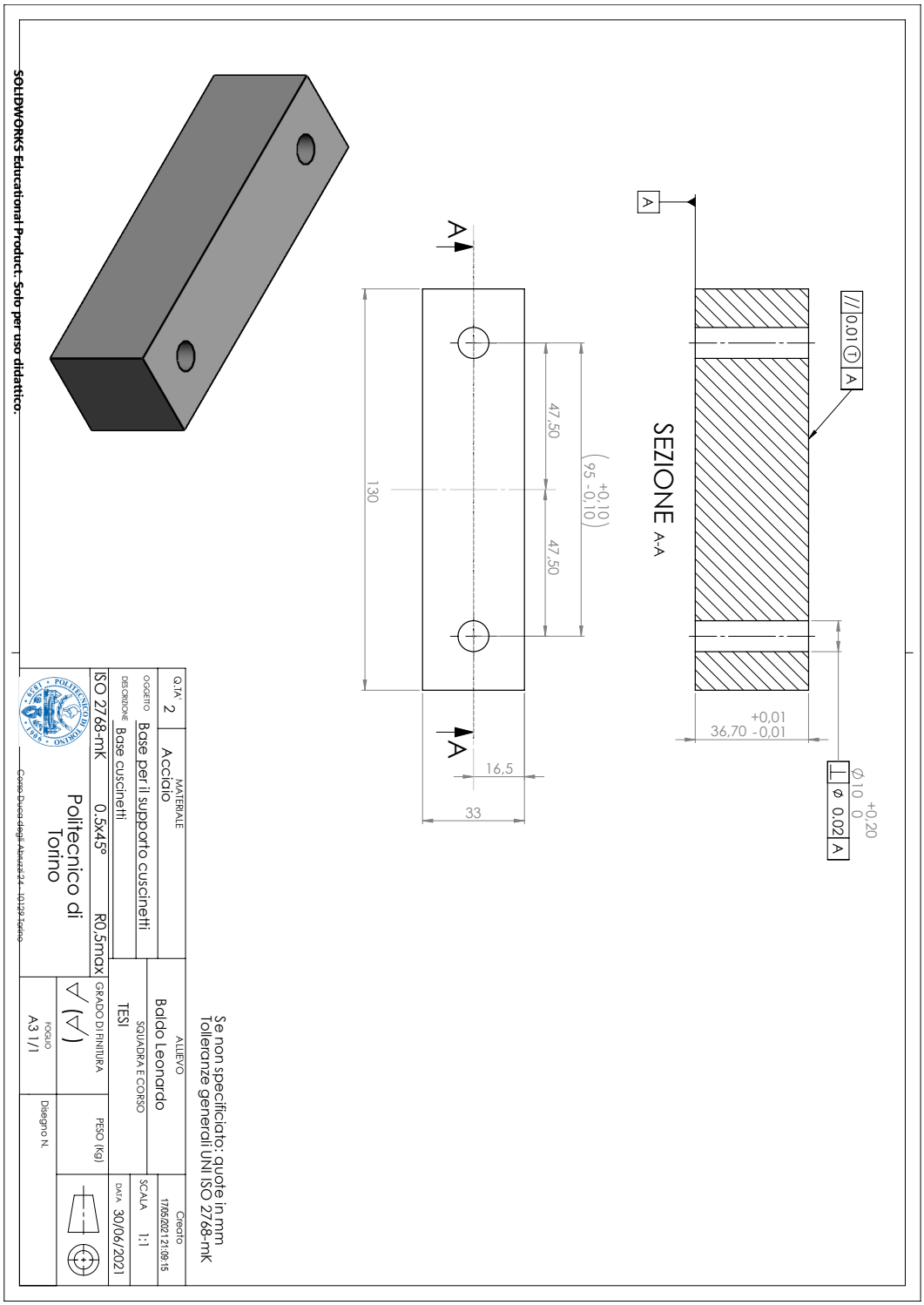
SEZIONE A-A
// 0.01 Ⓣ A
A
⊥ Ø 0.02 A
Ø10 +0,20 0
+0,01 36,70 -0,01
47,50
47,50
(95 +0,10 -0,10)
130
16,5
33
Se non specificato: quote in mm
Tolleranze generali UNI ISO 2768-mK
Q.TA' 2
MATERIALE Acciaio
OGGETTO Base per il supporto cuscinetti
DESCRIZIONE Base cuscinetti
ISO 2768-mK 0.5x45° R0,5max
GRADO DI FINITURA
PESO (Kg)
ALLIEVO Baldo Leonardo
SQUADRA E CORSO TESI
Creato 17/05/2021 21:09:15
SCALA 1:1
DATA 30/06/2021
Politecnico di Torino
Corso Duca degli Abruzzi 24 - 10129 Torino
FOGLIO A3 1/1
Disegno N.
SOLIDWORKS Educational Product. Solo per uso didattico.

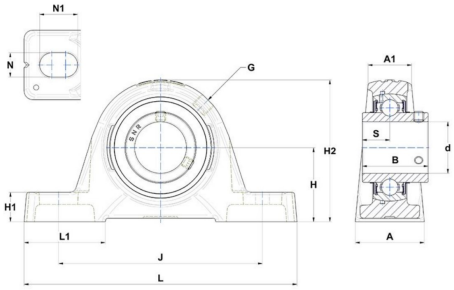

A	32 mm
A1	19 mm
B	31 mm
d	20 mm
H	33,3 mm
H1	14,5 mm
H2	64 mm
J	97 mm
L	130 mm
L1	40 mm
N	11 mm
N1	19 mm
S	12,7 mm

Figure 3.18: SNR bearing dimensions.

Weight	$0.57kg$
C	$12.8kN$
C_0	$6.65kN$
T_{min} T_{max}	$-20°C$ $+100°C$
Material	Cast iron
Bearing S/N	PE204

3.5.5 Elastic coupling.

An elastic coupling has been installed on the test bench to ensure a correct mechanical link between the output shaft of the gearbox and the main shaft of the test bench. An elastic coupling is always used in these application for joining two rotating part since, for manufacturing tolerances, the perfect alignment of mechanical components cannot be assured. In this case a special kind of coupling is needed with different input and output diameters to fulfill interface requirements with other components: $8mm-20mm$. The type of coupling we decided to purchase is called *"Jaw coupling"*. They are made of steel and they provide high torsional rigidity, thus not interfering with the load transfer to the gears' teeth. They present a locking mechanism with both mechanical keys and grub screws. Four coupling were purchased.

Figure 3.19: Mechanical elastic coupling.

3.5.6 External link ("Cup").

This mechanical component is needed to house the gearbox to be tested, which is installed with four threaded M3 bores on the superior part of the "Cup". The central area is slightly thicker to ensure a correct centering between this component and the gearbox. On the lateral, external flange other 4 holes permit the installation of this component to the support trough the same 4 bolts used for the motor (notice the same geometrical and dimensional tolerance).
Particular care has been put into the design of this mechanical piece, which has seen lots of versions and modification. More complex and simpler solutions were taken into consideration, such as installing centering bearings. However this solution is chosen as it is simple, quite reliable, easy to handle without specific equipment, more cost-effective and it does not pose threat concerning viscous friction. In fact, if on the one hand, adding more bearing would have surely improved the reliability of the mechanism, on the other hand, it would have added two main source of viscous friction, very difficult to model and to calculate just on the motor shaft. In the context of creating prognostic models this is unacceptable and it would have interfered with the quick "back and forth" movement needed to break down the gearboxes. In fact, inside of it, the motor shaft is connected to the geared link which is, de facto, the sun of the gearbox assembly without any external support.
In this way the "cup" serves as a spacer between the motor and the gearbox as Figure 3.2 clearly shows.
Added chamfers and fillets on the internal and external edges make the component lighter and easier to handle. This is the only component which has no important structural load and, as such, the material can be steel or also alluminium, easier to manufacture.

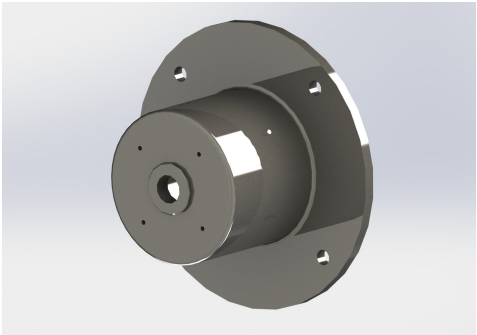

Figure 3.20: External "cup".

Despite the negligible structural loads the "cup" must bear (just the net torque due to the friction inside the bearing), this piece is very important indeed, as it links the input and the output of the gearbox. Since it has a pivotal role, tolerance must be placed with much care: two parallelism tolerances are placed on the surface in contact with the gear box while a concentricity tolerance is placed on the thicker part designed for the gearbox centering. j6 tolerance is placed on the ring used to center the "cup" on the support, while special tolerances are placed where the gearbox has to be centered. Roughness indications and dimensional tolerances complete the 2D drawing, shown in the next page.

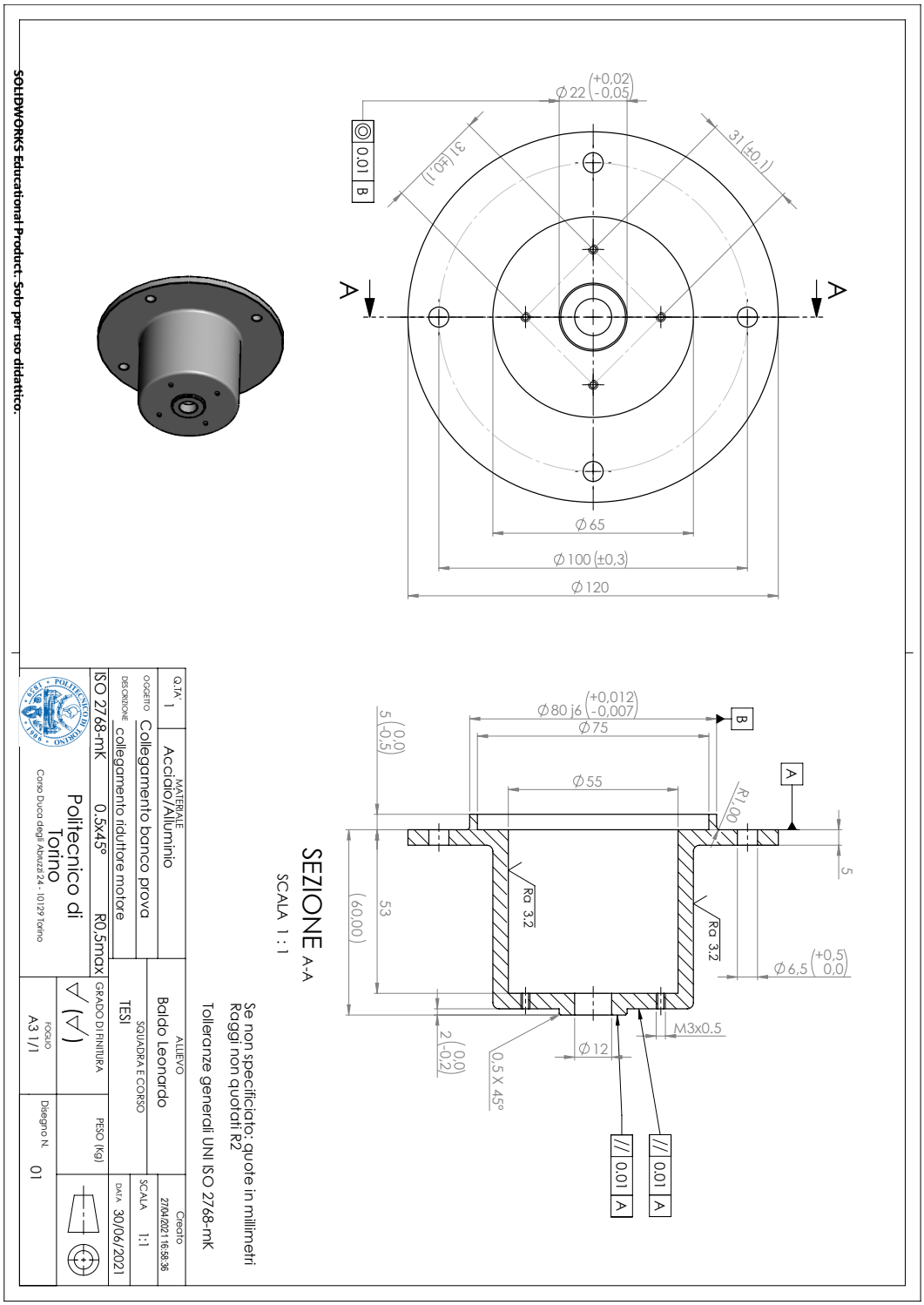
SOLIDWORKS Educational Product. Solo per uso didattico.
Ø22 (+0,02 -0,05)
0.01 B
31 (±0,1)
31 (±0,1)
A
A
Ø65
Ø100 (±0,3)
Ø120
SEZIONE A-A
SCALA 1 : 1
Ø80 j6 (+0,012 -0,007)
Ø75
Ø55
5 (0,0 -0,5)
B
A
R1,00
5
Ra 3.2
Ra 3.2
53
(60,00)
Ø6,5 (+0,5 0,0)
M3x0.5
Ø12
2 (0,0 -0,2)
0,5 X 45°
// 0.01 A
// 0.01 A
Se non specificato: quote in millimetri
Raggi non quotati R2
Tolleranze generali UNI ISO 2768-mK
Q.TA' 1
MATERIALE Acciaio/Alluminio
OGGETTO Collegamento banco prova
DESCRIZIONE collegamento riduttore motore
ISO 2768-mK 0.5x45° R0,5max
ALLIEVO Baldo Leonardo
SQUADRA E CORSO TESI
GRADO DI FINITURA
PESO (Kg)
Creato 27/04/2021 16:58:36
SCALA 1:1
DATA 30/06/2021
Disegno N. 01
FOGLIO A3 1/1
Politecnico di Torino
Corso Duca degli Abruzzi 24 - 10129 Torino

3.5.7 Main shaft.

The main shaft is a $20mm$ diameter steel shaft with special features. It links the output shaft of the gearbox (trough the elastic joint) and the flange with the flywheel attached.
The shaft diameter is standard thus reducing costs and general complexity.
As already explained, the shaft is sustained by the two bearing supports which keep it firmly in place with the grub screws.
The locking mechanism between this component and the flange is noteworthy. In fact, at the end of the shaft a threaded bore and a Seeger ring housing is envisaged. Trough the Seeger ring and a nut with a washer, the flange is longitudinally fixed onto the shaft.
In order to lock the flange in place, a key seat is designed onto the shaft.
The distance between the end of the shaft and the Seeger ring seating is carefully chosen to be some millimeters smaller than the length of the flange. In this way, by screwing in the nut at the end of the shaft, the flange will be pressed in place.
The length of $345mm$ is selected taking into account the general encumbrance of the bench and the possibility of testing gearboxes with different lengths, thus enabling the cross travel of the shaft along its longitudinal axis.
No particular tolerances are required, since these kinds of components are purchased already correctly measured and only relatively small rectifying procedures must be put in place.
General rugosity and dimensional tolerances are accurately designed (e.g. the distance between the end of the shaft and the Seeger ring seating must not be higher than selected otherwise the flange cannot be pressed). The h6 shaft tolerance is a standard value and is chosen so that every other component which have to interface with the shaft can be designed according to standard shaft-bore tolerances value.
Cylindricity and straightness tolerances of the external surface and of the central axis are implemented. The selected Seeger ring, typical for 20mm shaft is of DIN 471 UNI 7435 type, while the key is a 6X6X30 DIN 6885 A. The 2D drawing is reported in the next page.

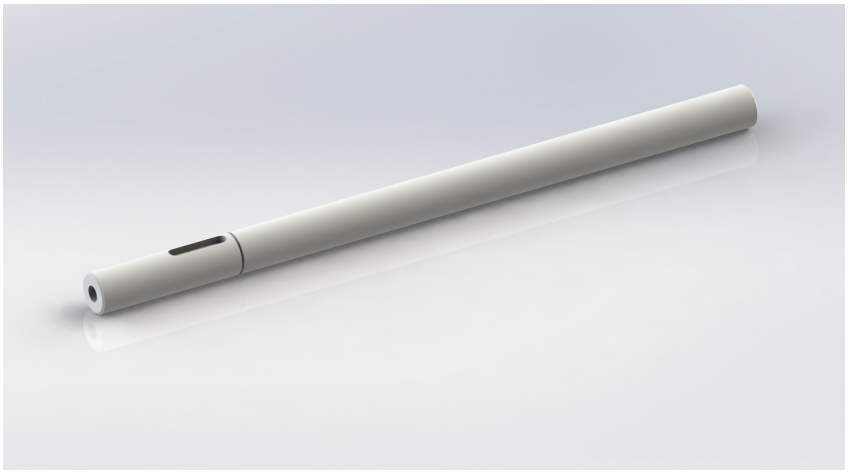

Figure 3.21: Main shaft.

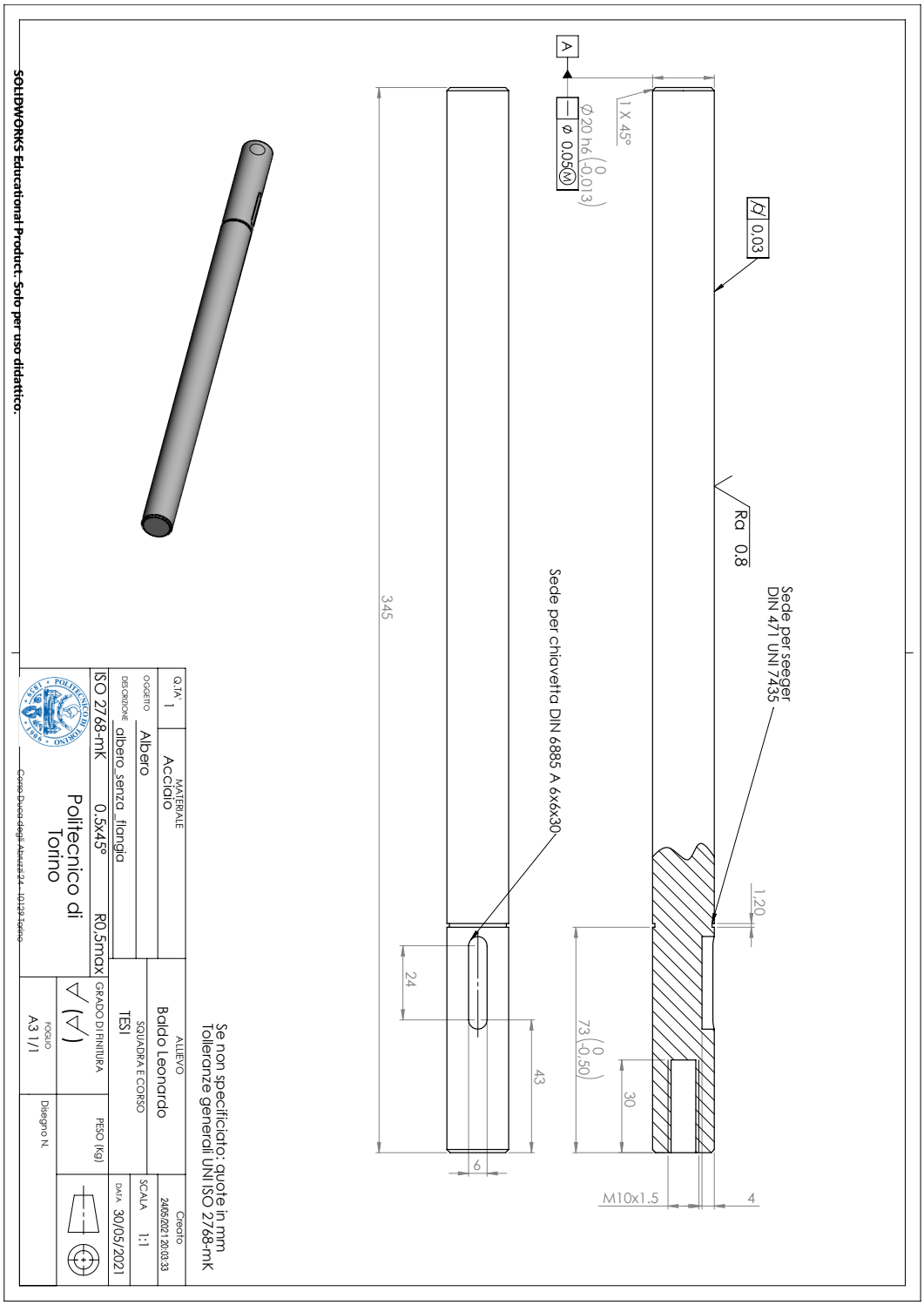
SOLIDWORKS Educational Product. Solo per uso didattico.
Se non specificato: quote in mm
Tolleranze generali UNI ISO 2768-mK
Sede per seeger
DIN 471 UNI 7435
Sede per chiavetta DIN 6885 A 6x6x30
Ø20 h6 (0 -0,013)
1 X 45°
0,03
Ra 0.8
345
24
43
6
1,20
73 (0 -0,50)
30
M10x1.5
4
Q.TA' 1
MATERIALE Acciaio
OGGETTO Albero
DESCRIZIONE albero_senza_flangia
ISO 2768-mK
0.5x45°
R0,5max
GRADO DI FINITURA
PESO (Kg)
ALLIEVO Baldo Leonardo
SQUADRA E CORSO TESI
SCALA 1:1
DATA 30/05/2021
Creato 24/05/2021 20:03:33
Politecnico di Torino
Corso Duca degli Abruzzi 24 - 10129 Torino
FOGLIO A3 1/1
Disegno N.

3.5.8 Flange.

The flange will be obtained from a turned steel block thanks to its longitudinal simmetry.
This component has the pivotal role of linking together the flywheel to the shaft providing enough resistance to withstand the inertial load of the flywheel.
Several particular features are present in this component:

- five threaded bores, useful to fix the flywheel. The tolerances, spacing and dimensions are the same as the one on the flywheel to ensure a correct mounting of the M12 nuts;
- a centering pin or spindle, necessary for the correct positioning of the flywheel which has to be centered precisely. Rugosity and g5 shaft tolerance are placed to correctly interface with the flywheel specifications. A $2X45°$ chamfer is also added to ensure an easy installation of the $22kg$ heavy flywheel;
- a key seat along the longitudinal length of the flange will house the key to firmly secure the flange on the shaft;
- fillets and chamfers;
- Cylindricity and concentricity tolerances on the centering pin;
- perpendicularity and circular runout tolerances on the vertical surface which has to mach with the flywheel surface;
- position tolerance with reference to reference feature A with the M modificator for the five threaded bores.

The 2D drawing is reported in the next page along with the renderings reported in Figure 3.22.

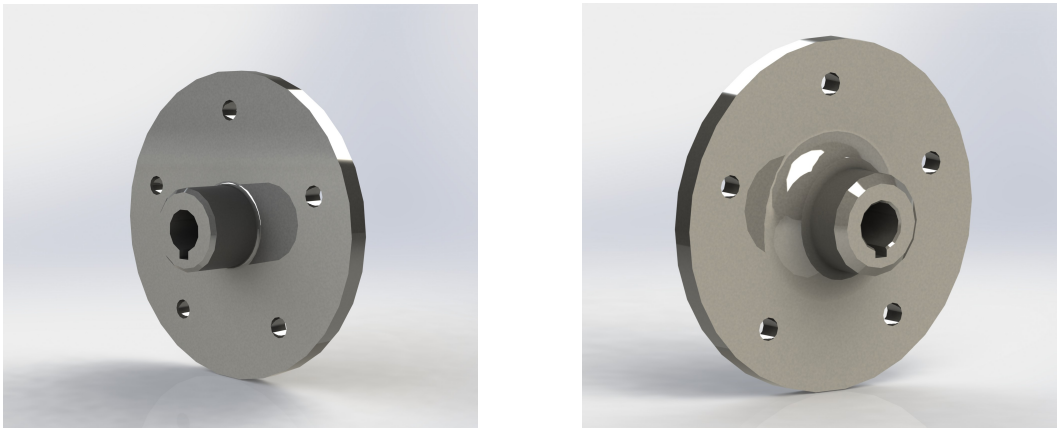

Figure 3.22: Flange rendering.

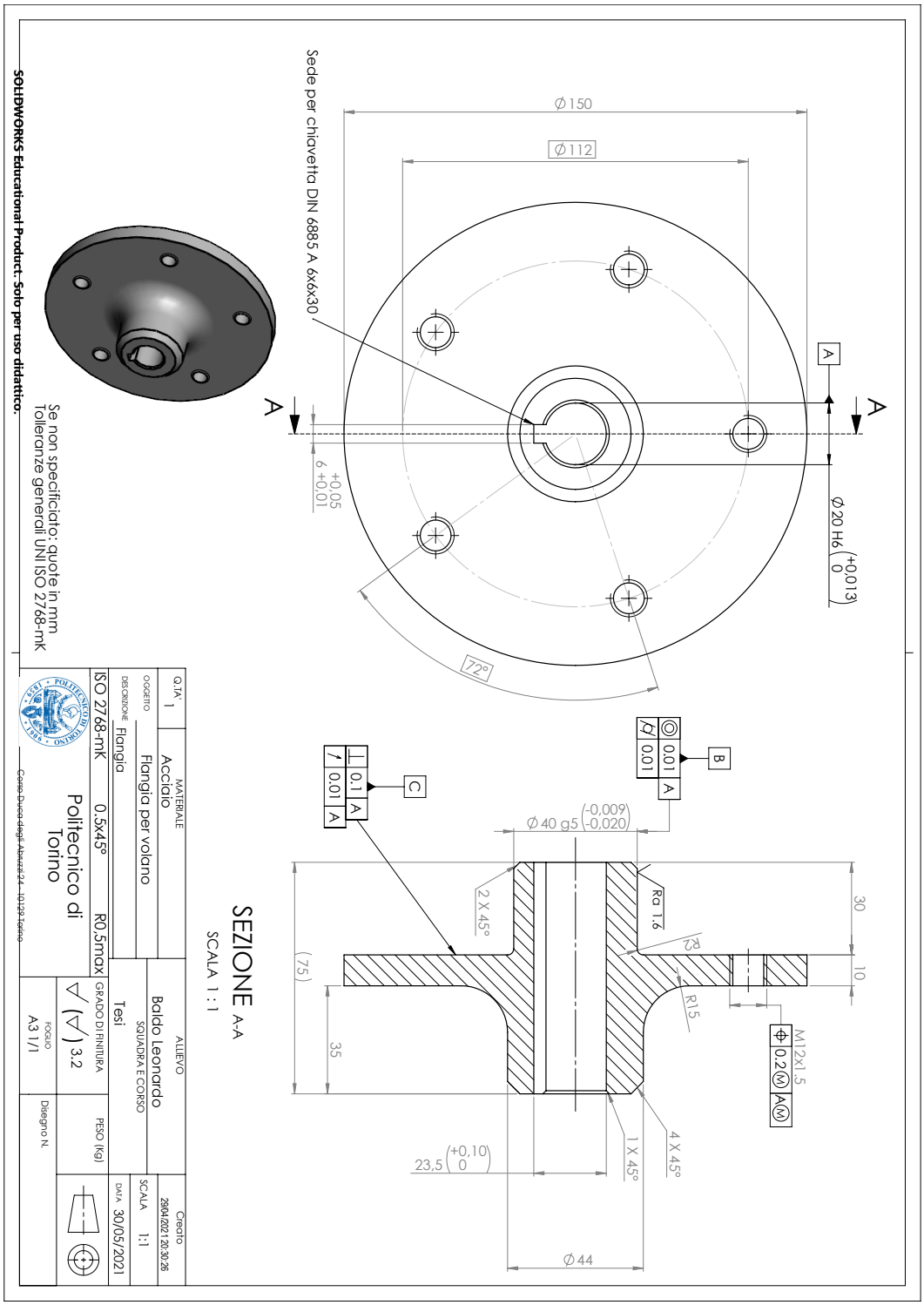
Sede per chiavetta DIN 6885 A 6x6x30
Ø150
Ø112
A
A
Ø 20 H6 (+0,013 0)
6 +0,05 +0,01
72°
B
C
0.01 A
0.1 A
0.01 A
Ø 40 g5 (-0,009 -0,020)
2 X 45°
Ra 1.6
30
10
R3
R15
(75)
35
M12x1.5
0.2 M A M
23,5 (+0,10 0)
1 X 45°
4 X 45°
Ø44
SEZIONE A-A
SCALA 1 : 1
Se non specificato: quote in mm
Tolleranze generali UNI ISO 2768-mK
SOLIDWORKS Educational Product. Solo per uso didattico.
Q.TA' 1
MATERIALE Acciaio
OGGETTO Flangia per volano
DESCRIZIONE Flangia
ISO 2768-mK 0.5x45° R0,5max
GRADO DI FINITURA ▽ (▽) 3.2
PESO (Kg)
ALLIEVO Baldo Leonardo
SQUADRA E CORSO Tesi
SCALA 1:1
DATA 30/05/2021
FOGLIO A3 1/1
Disegno N.
Creato 29/04/2021 20:30:26
Politecnico di Torino
Corso Duca degli Abruzzi 24 - 10129 Torino

3.5.9 Encoder and its 3D printed support.

The selected encoder is a CALT GHH80-20G2500BMP526 hollow shaft incremental rotary encoder.
Its main feature are: $5 - 26V$ power in, $20mm$ E7 bore, Interface with cables, 2500 pulse rate, Push pull logic.
More mechanical and general specification are reported in figure 3.25, while a picture of the encoder and the CAD model representing it are reported if figure 3.24. The tether has been created with the sheet metal tool offered by *Solidworks*, which made the design of this piece easier and significantly quicker.
See previous chapter for encoder working principles.

Figure 3.23: Encoder and its CAD model.

To secure the encoder, a CAD support has been designed. The support will be produced in PLA via additive manufacturing FDM technique. This component provides two holes for the encoder tether and a base to be fixed on the main bench steel support with two nuts.

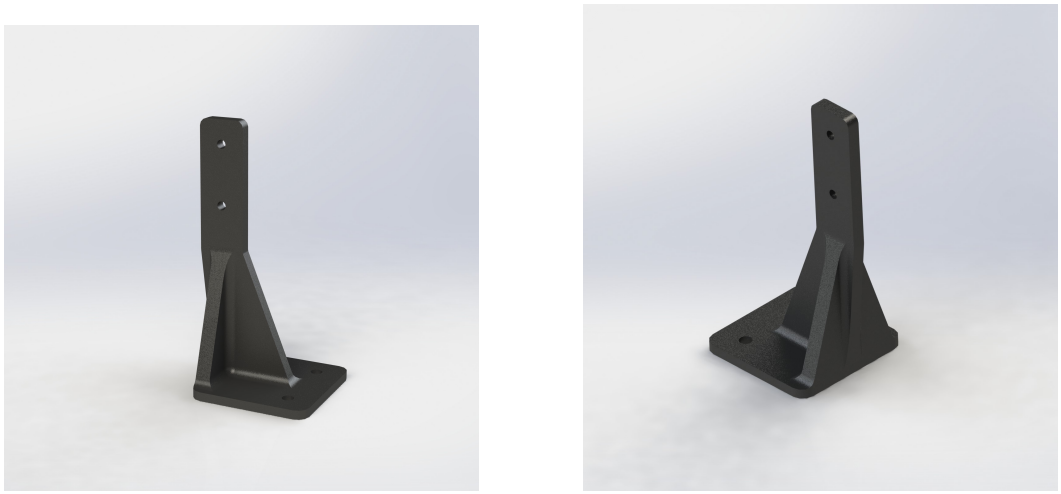

Figure 3.24: Encoder support CAD representation.

Electrical spec:

Output circuit	Open-collector output	Voltage output	Push-pull complementary outputs	driver
Supply voltage	5~30V	5~30V	5±0.25 5~30V	5±0.25 5~30V
Current consumption	≤80mA	≤80mA	≤80mA	≤150mA
Load current	40mA	40mA	40mA	60mA
Output high	Min Vcc*70%	Min Vcc-2.5V	Min Vcc-1.5V	Min 3.4V
Output low	MAX 0.4V	MAX 0.4V	MAX 0.8V	MAX 0.4V
Rise time Tr	MAX 1us	MAX 1us	MAX 1us	MAX 200ns
Fall time Tf	MAX 1us	MAX 1us	MAX 1us	MAX 200ns
Highest frequency response	300kHz	300kHz	300kHz	300kHz

Mechanical spec:

Max speed r/min	Starting torque	Axis maximum load	Impact	Anti-vibration
6000	<0.05Nm	Radial 25 N Axial 15N	50G/11ms	10G 10-2000Hz
Moment inertia	Work Temperature	Storage Temperature	Protection Degree	Weight
4 x 10.-8kgm²	-40~85℃	-40~85℃	IP50	400g

Dimensions :

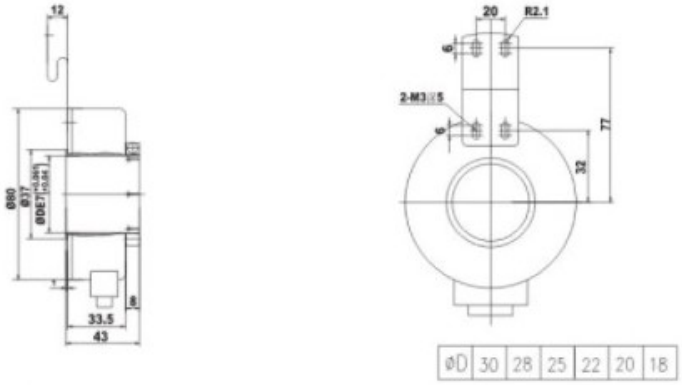

Output phase shift

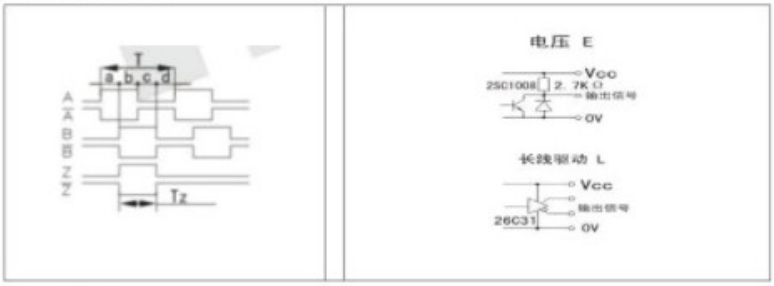

Connections:

Signal	A	B	Z	A-	B-	Z-	Vcc	GND
Color	Green	White	Yellow	Brown	Grey	Orange	Red	Black
Without inverted signal	Green	White	Yellow	-	-	-	Red	Black

Figure 3.25: Encoder specs.

3.5.10 Internal coupling.

The internal coupling engages on the output motor shaf twhile, at the other end, a geared section meshes with the planetary gearbox satellites.
This component saw different versions, mainly with length differences; this version is shorter than the other ones, providing the best trade off between costs, manufacturing issues and performances. In fact, this unit can be considered part of the gearbox assembly in the breaking test and, as such, it must be designed with particular care. In this sense, if this component will break down, it is considered as part of the gearbox assembly and the test will be considered legit. A total of 5 components has been ordered.
The spur gear parameters have been chosen accurately according with the ones on the gearboxes:

Spur gear data	
Modulus	0.5
Number of teeth	17
Pressure angle	2°
Addendum	$0.5mm$
Dedendum	$0.625mm$

Table 3.9: Spur gear data.

The extrusion cut on *Solidworks* has taken into account the gear generator, providing the visual representation of the undercuts.
A key seat has been placed according to the motor 2D drawings and a M4 threaded hole for a grub screw has been placed to firmly fix the component in place.
The 2D drawing is reported on the next page.

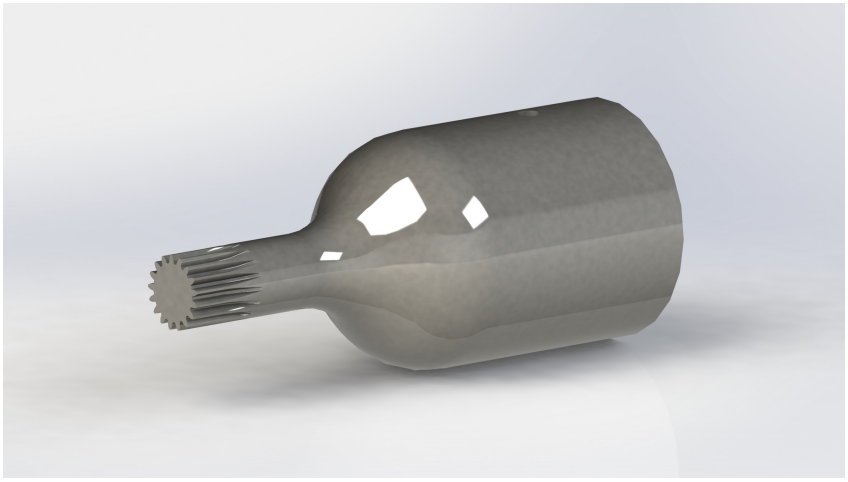

Figure 3.26: Internal coupling with spur gear.

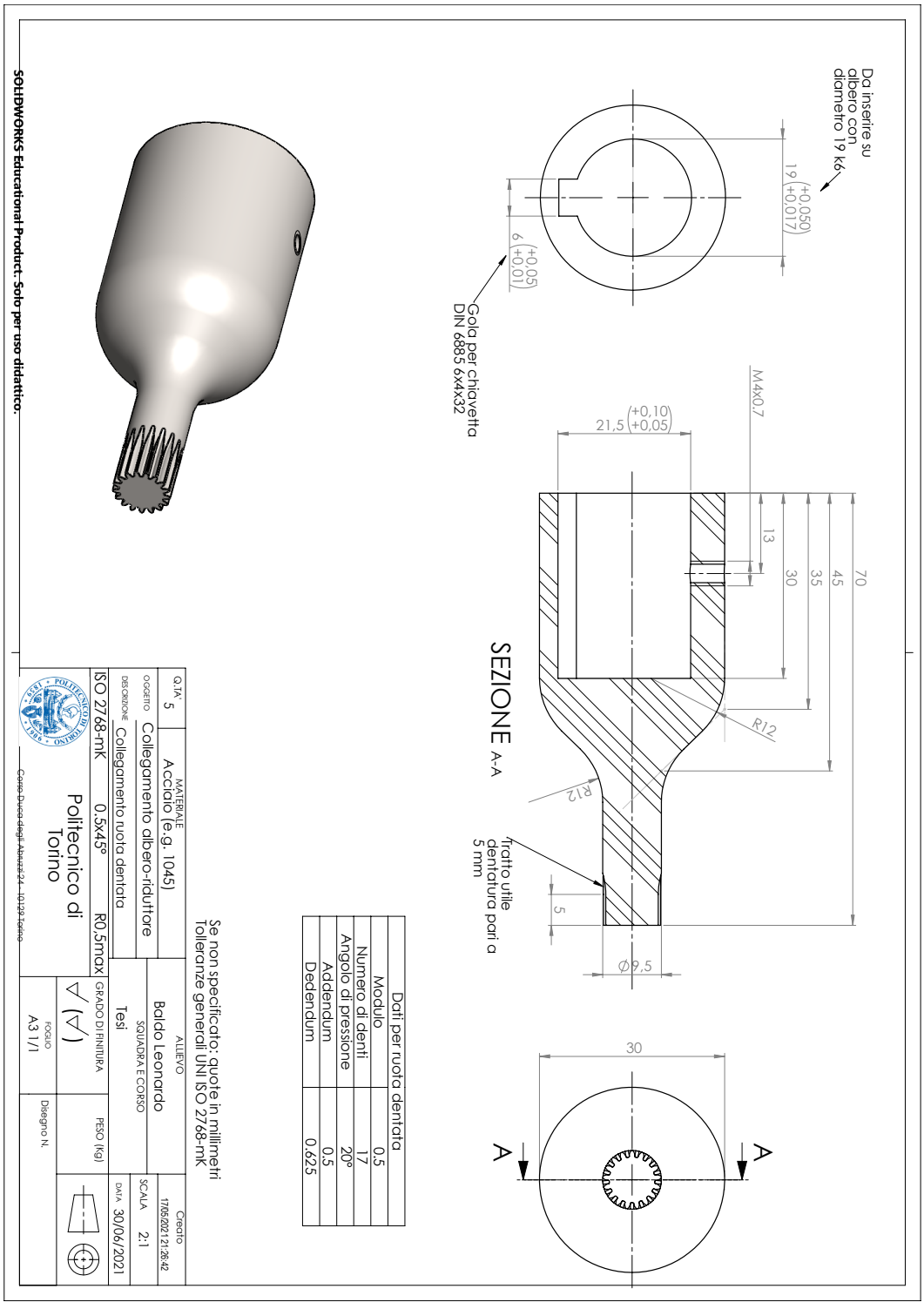
Da inserire su albero con diametro 19 k6
19 (+0,050 +0,017)
6 (+0,05 +0,01)
Gola per chiavetta DIN 6885 6x4x32
M4x0.7
21,5 (+0,10 +0,05)
13
30
35
45
70
R12
R12
SEZIONE A-A
Tratto utile dentatura pari a 5 mm
5
Ø9,5
30
A
A
Dati per ruota dentata
Modulo 0,5
Numero di denti 17
Angolo di pressione 20°
Addendum 0,5
Dedendum 0,625
Se non specificato: quote in millimetri
Tolleranze generali UNI ISO 2768-mK
Q.TA' 5
MATERIALE Acciaio (e.g. 1045)
ALLIEVO Baldo Leonardo
Creato 17/05/2021 21:26:42
OGGETTO Collegamento albero-riduttore
SQUADRA E CORSO Tesi
SCALA 2:1
DESCRIZIONE Collegamento ruota dentata
DATA 30/06/2021
ISO 2768-mK 0.5x45° R0,5max
GRADO DI FINITURA
PESO (Kg)
Politecnico di Torino
FOGLIO A3 1/1
Disegno N.
Corso Duca degli Abruzzi 24 - 10129 Torino
SOLIDWORKS Educational Product. Solo per uso didattico.

3.6 Assembly.

The final assembly 2D drawing is reported in the next page and it shows all the necessary details for the production phase and for a more in depth understanding of the test bench and of the concept behind it.
Thanks to cut views, the flywheel locking system is clearly visible: the key between the shaft and the flange, the Seeger ring, the nut and the washer are distinctively noticeable.
The "cup" and the internal coupling can be seen thanks to another cut view with the grub screw, the key and the gearbox assembly.
The bill of materials shows the type of screws, nuts, washers, mechanical keys etc along with their quantities.
The lateral view has been very useful to understand the overall dimensions of the test bench, to assess the project feasibility and to foresee each component interfaces with the other ones. For instance, thanks to interference studies and thanks to the assembly view helped me every time to come up with cleverer and smarter ideas.
One example is the concept of moving the flywheel assembly with the shaft attached to house gearboxes with different lengths without moving the entire bench assembly, thus reducing sure interface problems and making the project more user-friendly.
Great effort has been put in making this test bench come alive in the most intuitive and simple way possible: many design iterations have been carried out to make the project simpler and easier to assemble, once the parts will be ready.
We paid a lot of care for the assembly phases, trying to imagine the steps needed to mount the "cup" and the internal coupling, the flywheel and the flange and so on.

3.6.1 An insight on company estimates.

In addition to the test bench design phase as stated by the thesis title, I decided to make a step further and start an informative campaign with different small companies which deal everyday with mechanical components and precision mechanical parts.
Even if not explicitly asked from the thesis tutor and advisors, I really cared about this developing step. First of all I wanted to seize the opportunity to see mechanical machines and to learn more about the mechanical treatments to which the components will be subjected.
Secondly I think that a good designer has to see with his own eyes the machines and has to touch with his hands the materials to really feel the project he is working on.
Finally I took the opportunity to learn more about the industrial reality of these company in my local area.
I managed to visit and share information with 4 companies: EPAPOWER S.R.L (Via Salvemini 23 - 28012 Cressa (NO)), DEMA SNC Officina Meccanica (via Salvemini, 25 - 28012 Cressa (NO)), Vinzia Fratelli S.p.a (Via Borgomanero, 121 - 28010 Briga novarese (NO)), OFFICINA MECCANICA FERRARI GIANMARIO (Via Ferrari, 14 - 28012 Cressa (NO)).
Sharing information with industries, with engineers and technical personnel involved every day in the design and production of mechanical components has given me strong inputs to improve my designs.

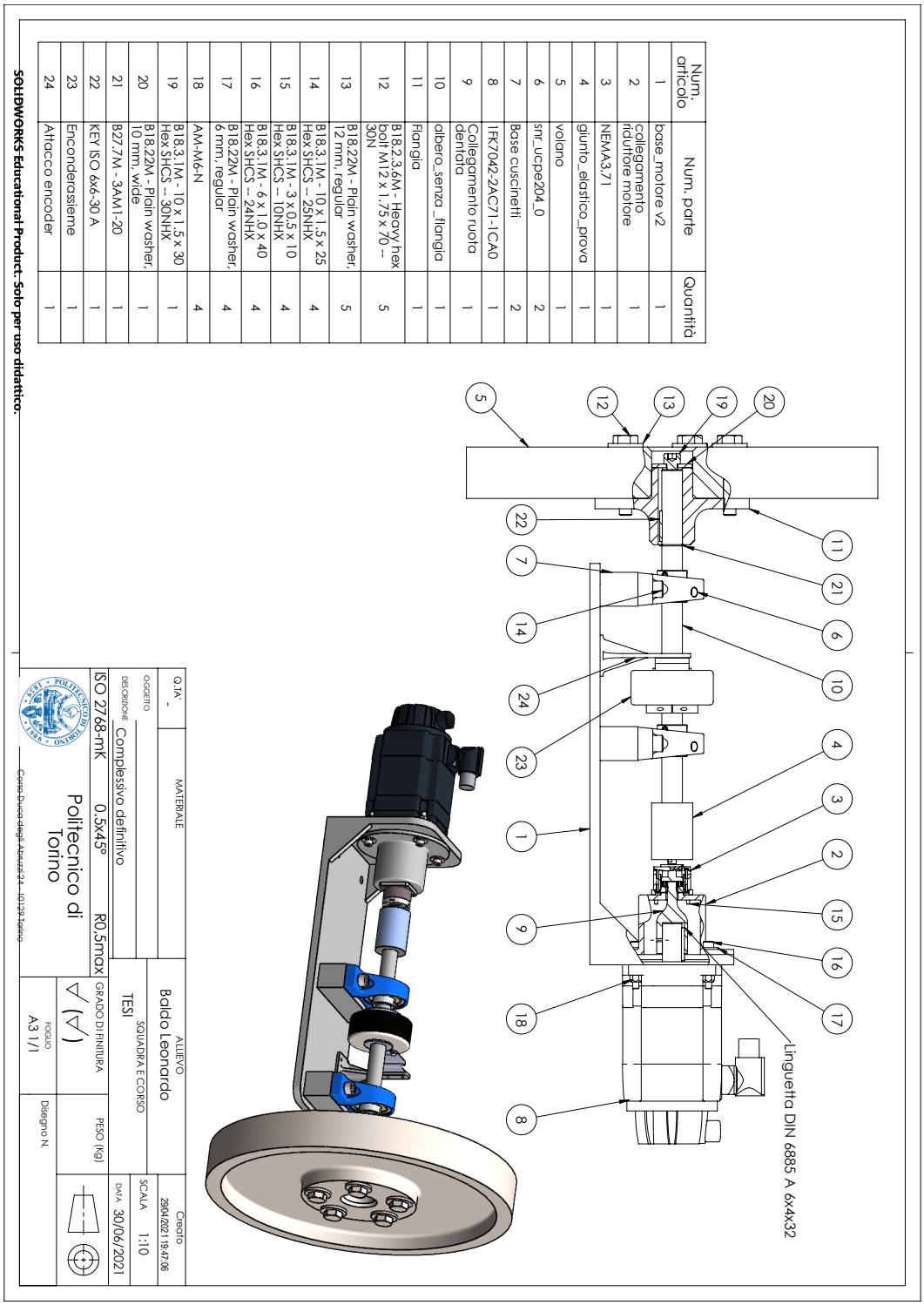

Num. articolo	Num. parte	Quantità
1	base_motore v2	1
2	collegamento riduttore motore	1
3	NEMA3,71	1
4	giunto_elastico_prova	1
5	volano	1
6	snr_ucpe204_0	2
7	Base cuscinetti	2
8	1FK7042-2AC71-1CA0	1
9	Collegamento ruota dentata	1
10	albero_senza_flangia	1
11	Flangia	1
12	B18.2.3.6M - Heavy hex bolt M12 x 1.75 x 70 -- 30N	5
13	B18.22M - Plain washer, 12 mm, regular	5
14	B18.3.1M - 10 x 1.5 x 25 Hex SHCS -- 25NHX	4
15	B18.3.1M - 3 x 0.5 x 10 Hex SHCS -- 10NHX	4
16	B18.3.1M - 6 x 1.0 x 40 Hex SHCS -- 24NHX	4
17	B18.22M - Plain washer, 6 mm, regular	4
18	AM-M6-N	4
19	B18.3.1M - 10 x 1.5 x 30 Hex SHCS -- 30NHX	1
20	B18.22M - Plain washer, 10 mm, wide	1
21	B27.7M - 3AM1-20	1
22	KEY ISO 6x6-30 A	1
23	Encoderassieme	1
24	Attacco encoder	1

3.6.2 An insight on tolerances.

Visualizing mates and interfaces between parts is an essential part of a forward-looking and conscious design, especially in mechanical components which will be manufactured by other industries or factories and where the main "spoken" language is trough technical drawings.
That is why I tried to foresee the mates and the problems which might arise once the pieces are going to be manufactured.
In this sense, Table 3.27 shows the desired results for each mates in terms of bore and shaft tolerances. I tried to use only standard GD & T dimensional and geometrical tolerances wherever possible. In the notes column some further information concerning the decision made is reported.

Mating elements	Bore	Shaft	Notes	Desired result
Motor-Motor and bench support	$80\ ^{+0.02}_{+0.012}$	$80\ j6\ 80\ ^{+0.012}_{-0.007}$	Centering	Tight loose/Loose
Motor-Internal coupler	$19\ ^{+0.05}_{+0.017}$	$19\ k6\ 80\ ^{+0.015}_{+0.002}$	With mechanical key and grub screw	Tight loose /Loose
External link "cup"-Motor and bench support	$80\ ^{+0.02}_{+0.012}$	$80\ j6\ 80\ ^{+0.012}_{-0.007}$	Centering	Tight loose /Loose
External link "cup"-Gearbox	$22\ ^{0}_{-0.15}$	$22\ ^{+0.02}_{-0.05}$	Centering	Loose
Main shaft-Elastic coupling	$20\ H6\ 20\ ^{+0.013}_{0}$	$20\ h6\ 20\ ^{0}_{-0.013}$	The coupling tightens	Tight loose
Main shaft-Bearing	$20\ ^{0}_{-0.01}$	$20\ h6\ 20\ ^{0}_{-0.013}$	With 2 grub screws	Tight loose
Main shaft-Encoder	$20\ E7\ 20\ ^{+0.061}_{+0.04}$	$20\ h6\ 20\ ^{0}_{-0.013}$	The encoder ring tightens	Loose
Main shaft -Flange	$20\ H6\ 20\ ^{+0.013}_{0}$	$20\ h6\ 20\ ^{0}_{-0.013}$	With mechanical key	Tight loose
Flange-Flywheel	$40\ H6\ 40\ ^{+0.016}_{0}$	$40\ g5\ 20\ ^{-0.009}_{-0.02}$	Centering	Tight loose

Table 3.10: Mates table.

Where one of the components involved in a mate is purchased as it is and not designed, (e.g. encoder, bearing, elastic joint...) the mate must be adherent with the factory tolerances.
The choice of a $20mm$ $h6$ was winning: this helped since it is a standard tolerance with which the encoder, the bearing, the elastic coupling and the flange can interface quite easily.
In fact, since h6 tolerances for a $20mm$ shaft are $+0$ in maximum material condition and -0.013 in minimum material condition, we can be sure that the shaft diameter will be always $\leq 20mm$. Following this decision, the encoder has an E7 tolerance which means that there will be always mechanical play between this electronic component and the shaft. However this is not a problem at all, since there are two grub screws keeping the encoder in place. Moreover, the mate between the shaft and the flange is desired as "tight loose", since there is a mechanical key, and, in fact, this can be accomplished quite easily with an H6 tolerance on the flange bore.

The connection between the flywheel and the flange centering pin is wanted "Tight loose", as commonly happens in centering hubs, and so a $g5/H6$ mate is accomplished.
Just in a few cases non-standard tolerances were selected: for instance in the *"motor-motor and bench support"* mate where the motor tolerance is taken from Siemens technical drawing and the support bore tolerance is chosen accordingly.
Finally also the tolerance concerning the internal coupling is non-standard since it must coexist with the motor shaft tolerance (See section 3.5.1 and technical drawings for the detailed tolerances).

3.6.3 Envisioned mounting sequence.

I tried to make this project the more user-friendly as possible since the beginning, hence I examined every possible solution to accomplish an easy to manufacture, easy to maintain, easy to mount bench.
On the other hand I also tried to conceive an assembly with as most standardized parts as possible to keep costs low but also to manufacture parts which can be reused in the most efficient way possible. In view of this lies the decision, already discussed (see Section 3.5.6), of not installing other bearings inside the "cup" to maintain the internal coupling centered. In fact, first of all there would have been the need of a bearing extractor tool and secondly those bearings would have been difficulty reused in other projects.
Another key aspect to remember is that this project will remain in the DIMEAS laboratory after my graduation, hence I tried to conceive a forward looking design which pays attention to prices and re usability opportunities.

In view of this considerations I am going to propose my prospect concerning the installation and assembly procedure. Obviously what I am proposing is my perspective of something that I cannot see in real life so probably there are going to be modifications to the procedure but I hope that the main instruction core may be useful anyway.

1. Position the *Motor and bench support* on the main table along with the bearing supports and the bearing support holders. Provide 6 holes in the table coincident with the holes on the main support, enabling the end of the shaft with the flywheel to protrude from the table.

2. Insert the 4 nuts in the bearing supports, in the supports holder, in the bench support and in the table, the holes should be coincident. Add other 2 nuts to firmly and definitely fix the main support at the table.

3. Install the motor and insert the four nuts without bolts.

4. now install the internal coupling with the mechanical key in such a way that it protrudes for some 5-6mm from the "cup" when it is mounted.

5. Now fix the gearbox to the "cup" and place the cup with the gearbox in its position. See in the internal coupling touches the internal part of the gearbox and if it meshes correctly with the gearbox satellites without friction. Regulate

the depth of the internal coupling accordingly and then fix it with the grub screw.

6. Now that the internal coupling is in the correct position without friction, the "cup" with the gearbox attached can be fixed with the four nuts, forming a "sandwich" with the motor and the main support.
7. It is now time to install the elastic coupling and secure it with grub screws.
8. The encoder support can now be anchored with two nuts to the main support.
9. The main shaft can be inserted from the end of the bench in the first bearing support, then in the encoder and finally in the second bearing support. It can be finally secured to the elastic coupling.
10. All grub screws can now be tightened and the encoder tether can be fixed to the 3D printed support.
11. The Seeger ring can now be installed on the main shaft as well as the second mechanical key in the key seat.
12. the flange can be installed following the key seat and fixed with a washer and a nut, screwed at the end of the main shaft.
13. The flywheel can now be installed following the centering pin and the five nuts can be screwed into the flange to secure it in place.

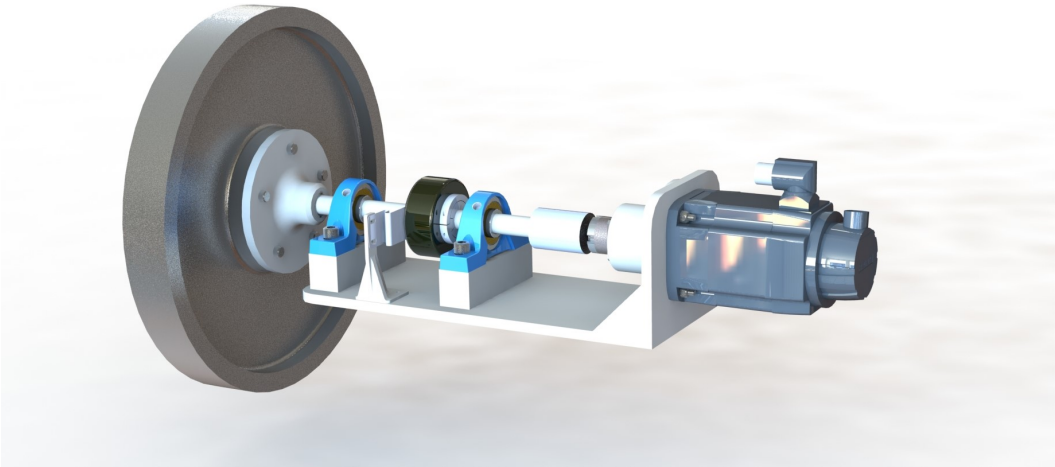

Figure 3.27: Another rendering of the test bench.

Chapter 4

Conclusions and future developments.

Working on this project made me grow up on many levels and helped me focus on my interests. Thanks to my initiative, I decided to bring this thesis a step forward not only looking after the parts design, which was the main point of the project, but also starting to handle the productive phases, making contacts with different industrial realities.
This effort has already paid off in different ways, speeding up the whole process and giving me a glimpse of the industrial environment which awaits me outside of the university.
I learned how to handle deadlines and how to deal with engineers already part of the industrial world. I gained experience on one of the main objective of a system engineer: handle conflicting requirements from many agents and providing a solution which best fits every request.
This has been challenging at times since I had to design an entire test bench from a bunch of requirements written on a sheet of paper. On the other hand, this opportunity of merging together a design and production point of view is the key of a forward looking design.

Of course this thesis provides just the initial step for a much bigger research work of algorithms validation and, more broadly, of PHM. This project had as its main goal arranging and handing over a test bench with a specified set of requirements with a set of experiments already in mind, but the possibilities of rearranging the components to validate different hypothesis or changing just some components and use the other in other ways are endless. In fact, this project blends in perfectly with nowadays systems engineering trends involving PHM and the overall increase of estimation methods for the RUL of electromechanical components. In this sense, future research should consider the potential effects of different kind of gearboxes and also testing the relevance of viscous friction relative to bearings.
Further developments could imply different "cups" for testing different kind of gearboxes but still exploiting the test bench platform, in this way the bench has been thought extremely modular and as simple as possible to operate.
Looking forward, further attempts and experiments based on the platform provided with this project could prove quite beneficial to the literature, enabling more data-

set useful for comparison and for research purposes.
As said before this is just the beginning of a much bigger research work; I am conscious this project still has a long way to go but I am confident that the well-reasoned solutions to many interfaces and general requirement related problems will be up to the challenges.

Appendix A

Bench previous design versions.

In order to get to the final design, many modifications and design iterations have been made on any component. In this chapter some older versions are presented, explaining why they were not selected at the end.
The most dramatic change concerns the general disposition of the main support which in first design phases was just for the motor itself and not for the bearing support. This revision has its roots in various reasons. The newer solution results in:

- a more stable and compact bench;
- guaranteed alignment between the parts, both longitudinally and laterally;
- less overall oscillations;
- small increase in material costs;
- possibility of mounting different length gearboxes without moving the motor (in the old version this happened thanks to slotted holes on the motor support) and thus not interfering with the goodness of the tests.

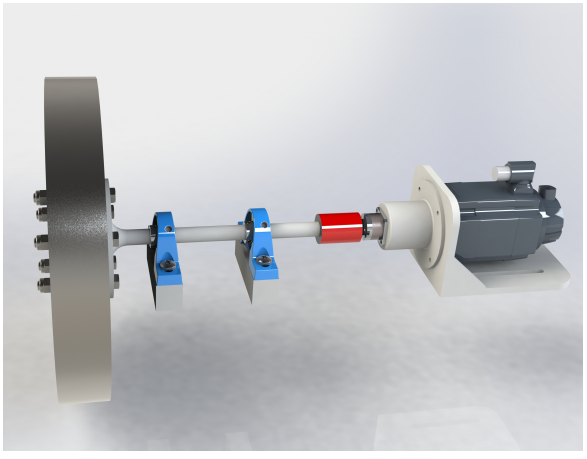

Figure A.1: Previous version with old shaft and old main support.

One of the other main design changes involves the main shaft and the flange. As visible in Figure B.1, in the first design stages the shaft and the flange were a single piece.
This had some major drawbacks:

- higher costs since the shaft and flange had to be extracted from a big single piece of metal;
- lack of centering pin for the flywheel;
- more complicated mounting procedure;
- more challenging preservation of strict tolerances;
- less compactness.

These design modifications came out during the useful and very productive meetings with engineers at the company EPAPOWER, where I received a lot of beneficial feedbacks.
Other less significant design revisions concerned: the internal coupling's length in order to limit lateral oscillations, the "cup" external and internal dimensions, the motor bracket's height and therefore the support's heights.
Furthermore the flywheel securing method and the centering pin have undergone major design changes, implementing the possibility of balancing the flywheel using tyre balancing machines, if necessary. This has been accomplished with the centering hole with a specific diameter and five holes with a specific diameter and in specific positions.

Appendix B

Experimental validation of gearboxes efficiency models.

B.1 Experimental setup

In the first period at DIMEAS facility, my colleagues and I carried out a parallel activity of acquiring data concerning gearboxes efficiency models.
These experimental reports were then exploited by eng. Pier Carlo Berri for his PhD dissertation. In this final appendix the results of those tests are reported, along with practical information about the tests and a validation with Simulink models performed by eng. Pier Carlo Berri himself.

The activity involved a small and temporary test bench made up of:

- a wooden table which provided support for the components;
- a brushed DC motor to provide torque;
- an high precision encoder (TSW581HS by Italsensor), already examined in section 2.2.1;
- wooden supports;
- a turned steel flange;
- some FDM made, PLA parts (e.g. winch, motor support, gearbox support etc);
- two pulleys with nylon rope;
- calibrated weights;
- a load-cell;
- three COTS gearboxes already examined in section 3.2
- control unit with potentiometer, double H-bridge and an Arduino UNO.

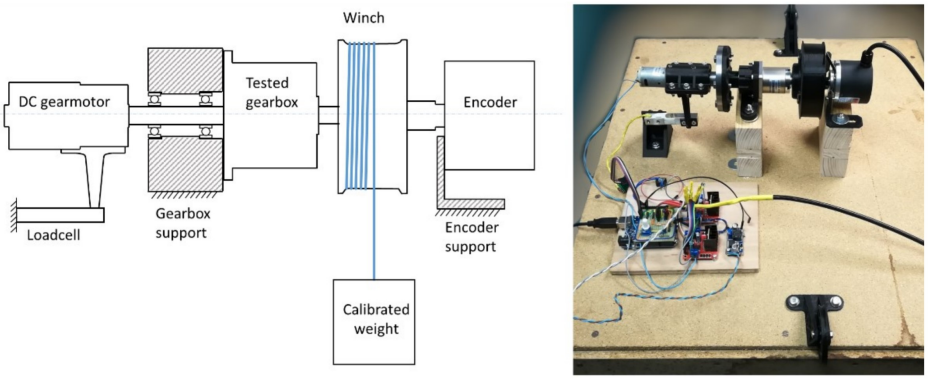

Figure B.1: Scheme and picture of the test bench.

The ultimate goal of the activity resulted from these acquired data is to validate simple but powerful models able to foresee mechanical transmission efficiency according to Berri et al. [1]. Similar validation (with an high fidelity model) is already present in literature but no experimental verification could be found.
The final results, better explained in Berri's PhD dissertation [21] shows coherent result and an astonishing prediction capability of these very simple (almost one equation) models.
The tests were conducted in aiding and opposing load conditions to achieve more exploitable data.
Experimental test were managed as follows: with the help of a Matlab script, data from the load cell and from the encoder were processed (with filters and post processing functions) and saved in log files.
The set of experimental trials are reported in the table below.

test	Load [grams]		
	LATO 1	LATO 2	Total
1	1555	1555	3110
2	1055	1055	2110
3	555	555	1110
4	1055	555	1610
5	1555	1055	2610
6	2055	1555	3610
7	555	55	610
8	55	55	110

Table B.1: Weights used in experimental tests.

According to different speed input values given trough the potentiometer knob (to get different data points), the torque and speed values were saved and then analysed (particular care was then taken to select time intervals with a constant speed in

[1] P. C. Berri, M. D. L. Dalla Vedova, P. Maggiore and A. Manuello Bertetto, "Simplified models for mechanical transmission efficiency with opposing and aiding loads," *International Journal of Mechanics and Control (JoMaC)*, vol. 20, no. 2, pp. 135-139, 2019.

order to reduce the inertial components in the torque). It goes without saying that the motor torque was obtained by multiplying the force times the distance from the load-cell to the motor shaft axis while the user torque could be obtained with the applied weight times the winch radius.
A winch with a smaller diameter was necessary when the load was very high.
The opposing/aiding load could be changed by varying the weights attached to the winch.

B.2 Theoretical background

An aiding load is the definition of a load connected to the user shaft of a mechanical device with helps the rotation of the output mechanism. In our case the aiding condition is visible when the calibrated weights are lowered (hence their weight helps the rotation of the output shaft).
On the other hand, an opposing load is encountered when the external load acts against the rotation of the output shaft under examination. In our case this condition takes place when the weights are lifted (hence their weight stands against the shaft rotation).
It is known that mechanical devices presents different efficiencies in the two conditions: this is mainly due to internal friction between gears. Usually the opposing load efficiency in multistage reduction mechanism η_D can be approximated as follows:

$$\eta_{D_{total}} = \left(\eta_{D_{singlestage}}\right)^{Numberofstages}$$

On the other hand the aiding load efficiency η_I is expected to decrease as the transmission becomes gradually irreversible.

According to the model exploited in [21] and firstly presented [22] it is possible to estimate the aiding load efficiency η_I knowing the opposing load efficiency η_D and the transmission ratio.

$$\eta_I = \frac{2\eta_D\tau - \tau + 1}{\eta_D\tau - \eta_D + 2} \tag{B.1}$$

In more details, equation B.1 is obtained, with some assumptions, from:

$$\eta_I = \tau \cdot \frac{T_{M,I}}{T_{U,I}} \tag{B.2}$$

where with $T_{M,I}$ and $T_{U,I}$ are reported the torques at the motor and user shafts in aiding load conditions. This simple equation is derived in [22] from friction and cinematic consideration. The main assumption made in [22] is considering that the link between η_I and η_D is mainly influenced only by the transmission ratio, disregarding the transmission architecture.
The results are now presented according to [21].

B.3 Results

After processing the acquired data, the results are plotted in Figures B.2 and B.3 concerning the first, second and third gearbox according to the table below.

	Gear ratio	**Number of stages**
Gearbox 1	3.71:1	1
Gearbox 2	13.73:1	2
Gearbox 3	50.89:1	3

Each figure shows the torque measured at the motor support plotted in function of the user torque (blue and red for opposing and aiding conditions respectively).
On each figure three lines are present: the first solid blue line fits the blue dots, which are the measured points.
The black dotted line represents the ideal condition with an efficiency equal to 1. In fact this line would be the exact bisector of cartesian graph if the gear ratio was equal to 1. Since the transmission ratio is not equal to 1, the line is angled according to the gear ratio (3.71 or 3.71^2 etc).
From the blue line η_D is estimated:

$$\eta_D = \left(\tau \cdot \frac{dT_m}{dT_l}\right)^{-1}$$

and, thanks to equation B.1, η_I is computed.
It is now possible to plot the red line:

$$T_m = \frac{T_l}{\tau} \cdot \eta_I - F$$

The red line is therefore the model of the aiding load condition efficiency which is able to foresee quite accurately the working point (dots in red). In other words, the red solid line, obtained thanks to the model explained in [22], fits with very good accuracy the experimental working points, despite the heavy assumption and the general simplicity of the model.
In some conditions the dots appear not exactly on the line due to the difficulties of tracking very low motor torques or due to the very high speed of the winch.
According to [21], the maximum error measured between the measured aiding load efficiency and the one estimated by the model is around 5 per cent, which is, once again, astonishing considering the straightforwardness of the model.

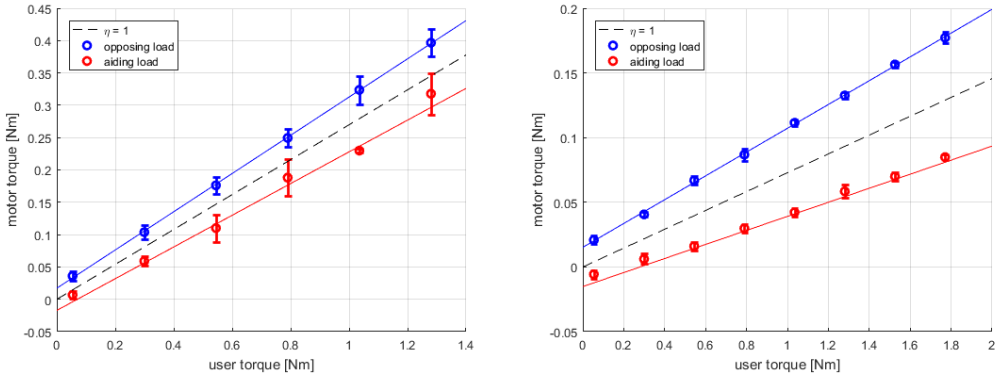

Figure B.2: Result for Gearbox 1 ($\tau = 3.71$) and Gearbox 2 ($\tau = 3.71^2$).

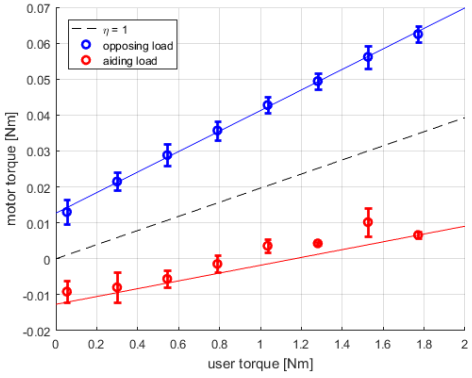

Figure B.3: Result for Gearbox 3 ($\tau = 3.71^3$).

Bibliography

[1] Ac induction motors vs. permanent magnet synchronous motors. *Web. https://empoweringpumps.com/ac-induction-motors-versus-permanent-magnet-synchronous-motors-fuji/.*

[2] Aisi 1045 medium carbon steel. *Web. https://www.azom.com/article.aspx?ArticleID=6130.*

[3] Brushless dc motor vs pmsm: Find out how these motors and their motor control solutions work. *Web. https://www.embitel.com/blog/embedded-blog/brushless-dc-motor-vs-pmsm-how-these-motors-and-motor-control-solutions-work.*

[4] C45 steel characteristics. *Web. https://steelpurchase.com/1045-s45c-c45-steel/.*

[5] Calt encoder cooperation advance liability trust. *Web. https://www.china-encoder.com/.*

[6] Design for manufacturing: Shaft keyways. *Web. https://www.wirebiters.com/dfm-shaft-keyway/.*

[7] Design for manufacturing: Turning small parts. *Web. https://www.wirebiters.com/dfm-shaft-keyway/.*

[8] Design of a flywheel. *Web. http://anandpgdie42.blogspot.com/2012/08/design-of-flywheel.html.*

[9] Induction vs. permanent magnet motor efficiency. *Web. https://www.horizontechnology.biz/blog/induction-vs-permanent-magnet-motor-efficiency-auto-electrification.*

[10] Linguette ad incastro uni 6604 din 6885. *Web. http://www.italchiavette.it/chiavette-uni-din-unificate/linguette-ad-incastro-uni-6604-din-6885/.*

[11] Ntn snr europe. *Web. https://www.ntn-snr.com/it.*

[12] Ntn snr industry general technical catalogue.

[13] Permanent magnet synchronous motor. *Web. https://www.theengineeringknowledge.com/permanent-magnet-synchronous-motor/.*

[14] Pla plastic material for 3d printing. *Web. https://www.sculpteo.com/en/materials/fdm-material/pla-material/.*

[15] Simotics s-1fk7 servomotors. *Web. https://new.siemens.com/global/en/products/drives/electric-motors/motion-control-motors/simotics-s/simotics-s-1fk7.html.*

[16] Supporto in ghisa - 2 fissaggi uspe204-snr. *Web. https://www.123cuscinetti.it/supporti-USPE204-SNR/container-tech-schema.*

[17] What is the difference between stator windings of bldc and pmsm motors? *Web. https://www.researchgate.net/post/What-is-the-difference-between-stator-windings-of-BLDC-and-PMSM-motors.*

[18] V. Atamuradov, K. Medjaher, P. Dersin, B. Lamoureux, and N. Zerhouni. Prognostics and health management for maintenance practitioners-review, implementation and tools evaluation. *International Journal of Prognostics and Health Management*, 8(060):1–31, 2017.

[19] S. Barella and A. Gruttadauria. *Metallurgia e materiali non metallici: teoria ed esercizi svolti.* Società Editrice Esculapio, 2017.

[20] P. Berri, M. Dalla Vedova, P. Maggiore, and A. M. Bertetto. High gear ratio mechanical transmissions for actuators: Simplified models for efficiency under opposing and aiding loads. In *IOP Conference Series: Materials Science and Engineering*, volume 1024, page 012097. IOP Publishing, 2021.

[21] P. C. Berri". "design and development of algorithms and technologies applied to prognostics of aerospace systems." PhD dissertation.

[22] P. C. Berri, M. Dalla Vedova, P. Maggiore, and A. Manuello Bertetto. Simplified models for mechanical transmission efficiency with opposing and aiding loads. *International Journal of Mechanics and Control*, 20(02):135–139, 2019.

[23] P. C. Berri, M. D. Dalla Vedova, P. Maggiore, and G. Riva. Design and development of a planetary gearbox for electromechanical actuator test bench through additive manufacturing. In *Actuators*, volume 9, page 35. Multidisciplinary Digital Publishing Institute, 2020.

[24] "Bolzern, Scattolini, and Schiavoni". *"Fondamenti di controlli automatici".* "Mc Graw-Hill", "2008".

[25] E. Bonisoli. "technical drawing", slides and lessons of the course. 2017.

[26] V. Boschetti". "development of an experimental test bench for the validation of prognostic algorithms for electromechanical actuators, 2020". Master's thesis.

[27] E. Chirone and S. Tornincasa. *Disegno tecnico industriale.* Il capitello, 1996.

[28] S. Derammelaere, M. Haemers, J. De Viaene, F. Verbelen, and K. Stockman. A quantitative comparison between bldc, pmsm, brushed dc and stepping motor technologies. In *2016 19th International Conference on Electrical Machines and Systems (ICEMS)*, pages 1–5. Ieee, 2016.

[29] T. Instrument. The difference between pmsm & bldc motor.

[30] G. Jacazio and B. Piombo. *Meccanica applicata alle macchine*. Levrotto & Bella, 1994.

[31] R. Jihin, D. Söffker, and N. Beganovic. Integrated prognostic model for rul estimation using threshold optimization. *Structural Health Monitoring 2017*, (shm), 2017.

[32] J. Li, Z. Yu, Y. Huang, and Z. Li. A review of electromechanical actuation system for more electric aircraft. In *2016 IEEE International Conference on Aircraft Utility Systems (AUS)*, pages 490–497. IEEE, 2016.

[33] Z. Lv, J. Wang, G. Zhang, and H. Jiayang. Prognostics health management of condition-based maintenance for aircraft engine systems. In *2015 IEEE Conference on Prognostics and Health Management (PHM)*, pages 1–6. IEEE, 2015.

[34] P. Maggiore. "sistemi di bordo aerospaziali", slides and lessons of the course. 2019.

[35] P. Maggiore. "modellazione, simulazione e sperimentazione dei sistemi aerospaziali", slides and lessons of the course. 2021.

[36] G. Qiao, G. Liu, Z. Shi, Y. Wang, S. Ma, and T. C. Lim. A review of electromechanical actuators for more/all electric aircraft systems. *Proceedings of the Institution of Mechanical Engineers, Part C: Journal of Mechanical Engineering Science*, 232(22):4128–4151, 2018.

[37] M. Repetto and S. Leva. Elettrotecnica. *Elementi di teoria ed esercizi. CittaStudi*, 2014.

[38] S. Sakunthala, R. Kiranmayi, and P. N. Mandadi. A study on industrial motor drives: Comparison and applications of pmsm and bldc motor drives. In *2017 International Conference on Energy, Communication, Data Analytics and Soft Computing (ICECDS)*, pages 537–540. IEEE, 2017.

[39] E. Sandgren and K. Ragsdell. Optimal flywheel design with a general thickness form representation. 1983.

[40] P. Sciandra". "development of an experimental test bench for the validation of prognostic algorithms for electromechanical actuators, 2020". Master's thesis.

[41] G. Szala and B. Ligaj. Application of hybrid method in calculation of fatigue life for c45 steel (1045 steel) structural components. *International Journal of Fatigue*, 91:39–49, 2016.

[42] Y. Tang, E. Lomonova, J. Paulides, and E. Kazmin. Investigation of winding topologies for permanent magnet in-wheel motors. 03 2014.

[43] G. J. Vachtsevanos and G. J. Vachtsevanos. *Intelligent fault diagnosis and prognosis for engineering systems*, volume 456. Wiley Online Library, 2006.

[44] P. Yedamale and D. Brushless. Motor fundamentals, microchip technology inc. *Application Note AN885*, 2003.